

Production of $K^*(892)^0$ and $\phi(1020)$ in pp collisions at $\sqrt{s} = 7$ TeV

The ALICE Collaboration*

CERN, 1211 Geneva 23, Switzerland

Received: 31 August 2012 / Published online: 30 October 2012

© CERN for the benefit of the ALICE collaboration 2012. This article is published with open access at Springerlink.com

Abstract The production of $K^*(892)^0$ and $\phi(1020)$ in pp collisions at $\sqrt{s} = 7$ TeV was measured by the ALICE experiment at the LHC. The yields and the transverse momentum spectra $d^2N/dydp_T$ at midrapidity $|y| < 0.5$ in the range $0 < p_T < 6$ GeV/c for $K^*(892)^0$ and $0.4 < p_T < 6$ GeV/c for $\phi(1020)$ are reported and compared to model predictions. Using the yield of pions, kaons, and Ω baryons measured previously by ALICE at $\sqrt{s} = 7$ TeV, the ratios K^*/K^- , ϕ/K^* , ϕ/K^- , ϕ/π^- , and $(\Omega + \bar{\Omega})/\phi$ are presented. The values of the K^*/K^- , ϕ/K^* and ϕ/K^- ratios are similar to those found at lower centre-of-mass energies. In contrast, the ϕ/π^- ratio, which has been observed to increase with energy, seems to saturate above 200 GeV. The $(\Omega + \bar{\Omega})/\phi$ ratio in the p_T range 1–5 GeV/c is found to be in good agreement with the prediction of the HIJING/B \bar{B} v2.0 model with a strong colour field.

1 Introduction

The study of resonance production plays an important role both in elementary and in heavy ion collisions. In pp and e^+e^- collisions it contributes to the understanding of hadron production [1, 2] as the decay products of resonances represent a large fraction of the final state particles. In addition, it provides a reference for tuning event generators inspired by Quantum Chromodynamics (QCD). In heavy ion collisions, resonances are a sensitive probe of the dynamical evolution of the fireball. Due to their short lifetime (a few fm/c) a significant fraction of resonances decay inside the hot and dense medium and their hadronic daughters interact with the medium during the fireball expansion [3–5].

The $\phi(1020)$, which is the lightest vector meson composed of sea quarks only, provides a probe for the study of the strangeness production. In pp collisions, $s\bar{s}$ pair produc-

tion was found to be significantly suppressed in comparison to $u\bar{u}$ and $d\bar{d}$ -pair [6, 7]. Another useful probe of strangeness production is the $K^*(892)^0$, which is a vector meson with a mass similar to the ϕ , but differing by one unit of the strangeness quantum number. The $(\Omega + \bar{\Omega})/\phi$ ratio has been suggested [8] as a probe of the colour field strength, which in microscopic models influences the relative yield of strange with respect to non-strange particles.

We present the first measurement of the differential ($d^2N/dydp_T$) and p_T -integrated (dN/dy) yields of the K^* ¹ and $\phi(1020)$ mesons at midrapidity ($|y| < 0.5$) in pp collisions at $\sqrt{s} = 7$ TeV. The data analysis was carried out for K^* (ϕ) on a sample of 80 (60) million minimum bias pp collisions collected by the ALICE experiment. The resonances were identified via their main decay channel $K^* \rightarrow \pi^\pm + K^\mp$ and $\phi \rightarrow K^+ + K^-$. Tracks were reconstructed by the main ALICE tracking devices, the Time Projection Chamber (TPC) and the Inner Tracking System (ITS). The TPC and Time of Flight (TOF) detectors were used to identify pions and kaons. The measured spectra are compared to two QCD-based event generators, PHOJET [9, 10] and PYTHIA [11].

The ratios K^*/K^- , ϕ/K^* , ϕ/K^- , and ϕ/π^- are computed using the yield of pions and kaons measured [12] with the ALICE detector in pp collisions at 7 TeV. These ratios are compared with measurements at lower collision energies. The $(\Omega + \bar{\Omega})/\phi$ ratio has been calculated as a function of transverse momentum using the Ω and $\bar{\Omega}$ yield measured at 7 TeV [13]; this ratio is then compared to the predictions of the HIJING/B \bar{B} v2.0 model with a Strong Colour Field (SCF) [14] and to PYTHIA-Perugia 2011 [15].

The article is organized as follows: Sect. 2 gives details about the detectors relevant for this analysis, Sect. 3 describes the criteria used for event selection, Sect. 4 gives an overview of the analysis, Sect. 5 presents the results and Sect. 6 the conclusions.

* e-mail: Angela.Badala@ct.infn.it

¹ We denote by K^* the average of $K^*(892)^0$ and $K^*(892)^+$.

2 Experimental set-up

A full description of the ALICE detector can be found in [16, 17]. For the analyses described in this paper, the ITS, the TPC, and the TOF detectors were used. These detectors are set inside a large solenoidal magnet providing a magnetic field $B = 0.5$ T, and have a common pseudorapidity coverage of $|\eta| < 0.9$. Two forward scintillator hodoscopes (VZERO) placed along the beam direction at -0.9 m and 3.3 m on either side of the interaction point, cover the pseudorapidity regions $-3.7 < \eta < -1.7$ and $2.8 < \eta < 5.1$. These are used for triggering and for rejecting beam-gas interactions.

2.1 The Inner Tracking System

The ITS [17] is the innermost ALICE detector, located between 3.9 and 43 cm radial distance from the beam axis. It is made of six cylindrical layers of silicon detectors (two layers of pixels, two of silicon drift, and two of silicon strips), with a total material budget of 7.66 % of the radiation length X_0 . It provides high-resolution space points close to the interaction vertex, thus improving momentum and angular resolution of the tracks reconstructed in the TPC.

The two innermost ITS layers constitute the Silicon Pixel Detector (SPD), which has a high granularity of about 9.8 million pixel cells, each with a size of $50 \times 425 \mu\text{m}^2$. These layers are located at radii of 3.9 and 7.6 cm with pseudorapidity coverages of $|\eta| < 2.0$ and $|\eta| < 1.4$, respectively. The detector provides a position resolution of $12 \mu\text{m}$ in the $r\phi$ direction and about $100 \mu\text{m}$ in the direction along the beam axis.

2.2 The Time Projection Chamber

The TPC [18] is the main ALICE tracking device. It is a large-volume, high-granularity, cylindrical drift detector which has a length of 5.1 m and inner and outer radii of 0.85 and 2.47 m, respectively. It covers the pseudorapidity range $|\eta| < 0.9$ with a full azimuthal acceptance. The drift volume is filled with 90 m^3 of $\text{Ne}/\text{CO}_2/\text{N}_2$. The maximum drift time is $94 \mu\text{s}$. A total of 72 multi-wire proportional chambers with cathode pad readout instrument the two end plates, which are segmented into 18 sectors and include a total of over 550,000 readout pads. The ionization electrons drift for up to 2.5 m and are measured on 159 pad rows. The momentum resolution of the TPC is in the range 1–7 % for pions with $1 < p_T < 10 \text{ GeV}/c$. The ALICE TPC ReadOut (AL-TRO) chip, employing a 10 bit ADC at 10 MHz sampling rate and digital filtering circuits, allows for precise position and linear energy loss measurements with a gas gain of the order of 10^4 . The material budget of the TPC near $\eta = 0$ amounts to about 4.1 % of X_0 .

The position resolution in the $r\phi$ direction varies between $1100 \mu\text{m}$ and $800 \mu\text{m}$ going from the inner to the outer radius, whereas the resolution along the beam axis varies between $1250 \mu\text{m}$ and $1100 \mu\text{m}$.

2.3 The Time Of Flight detector

The ALICE TOF [19, 20] is a cylindrical assembly of Multi-gap Resistive Plate Chambers (MRPC) with an inner radius of 370 cm and an outer radius of 399 cm. It has a pseudorapidity coverage of $|\eta| < 0.9$ and full azimuthal acceptance, except for the region $260^\circ < \phi < 320^\circ$ at $|\eta| < 0.14$ where a gap was left in order to reduce the amount of material in front of the Photon Spectrometer (PHOS). The elementary unit of the TOF system is a 10-gap double-stack MRPC strip 122 cm long and 13 cm wide, with an active area of $120 \times 7.4 \text{ cm}^2$ subdivided into two rows of 48 pads of $3.5 \times 2.5 \text{ cm}^2$ each. The length of the TOF barrel active region is 741 cm. It has about 153,000 readout channels and an average thickness of 25–30 % of X_0 , depending on the detector zone. For pp collisions, such a segmentation leads to an occupancy below 0.02 %. The front-end electronics are designed to comply with the basic characteristics of the MRPC detector, i.e. very fast differential signals from the anode and the cathode readout: the resulting intrinsic time resolution of the detector and electronics was measured to be smaller than 50 ps.

3 Data collection and event selection

Data used for this analysis were collected in 2010 using a magnetic field of $B = 0.5$ T with both field polarities. The minimum bias trigger required a single hit in the SPD detector or in one of the two VZERO counters, i.e. at least one charged particle anywhere in the ~ 8 units of pseudorapidity covered by these detectors. In addition, a coincidence was required with signals from two beam pick-up counters, one on each side of the interaction region, indicating the passage of proton bunches. The trigger selection efficiency for inelastic collisions was estimated to be 85.2 % with a +6.2 % and -3 % uncertainty [21]. During the data-taking period, the luminosity at the ALICE interaction point was kept in the range $0.6\text{--}1.2 \times 10^{29} \text{ cm}^{-2} \text{ s}^{-1}$. Runs with a mean pile-up probability per event larger than 5 % were excluded from the analysis.

Beam-induced background was reduced to a negligible level (< 0.01 %) with the help of the timing information of the VZERO counters and by a cut on the position of the primary vertex reconstructed by the SPD [22]. Accepted events were required to have a reconstructed primary vertex. Its position can be computed either using the tracks reconstructed by TPC and ITS, or using the “tracklets” obtained connecting reconstructed clusters in both SPD layers. If possible, the

first method is used. First, for each event a three dimensional reconstruction of the primary vertex was attempted with either a Kalman filter, using reconstructed tracks as input, or by a minimization of the squared distances between all the extrapolated tracklets. Otherwise only the z position of the primary vertex was reconstructed by correlating the z coordinates of the SPD space points, while for x and y the average position of the beam in the transverse plane was taken. The primary vertex reconstruction efficiency, calculated via Monte Carlo simulation, approaches unity in events with a K^* or a ϕ produced in the central rapidity region. In order to minimize acceptance and efficiency biases for tracks at the edge of the TPC detection volume, events were accepted only when their primary vertex was within ± 10 cm from the geometrical centre of the ALICE barrel.

4 Data analysis

4.1 Track selection

Global tracking in ALICE is performed using ITS and TPC clusters. It is based on a Kalman filter algorithm which takes into account both multiple scattering and energy loss along the path as described in detail in [23]. The Distance of Closest Approach (DCA) to the primary vertex is used to discriminate between primary and secondary particles. Primary charged particles are those produced directly in the interaction and all decay products from particles with a proper decay length $c\tau < 1$ cm; secondary particles include those from the weak decay of strange hadrons and from interactions in the detector material. Several cuts were applied to achieve a high track quality in the analyzed sample. Tracks were required to have at least 70 reconstructed clusters in the TPC out of the maximum 159 available. This ensured a high efficiency and good dE/dx resolution, keeping the contamination from secondary and fake tracks small.

In order to improve the global resolution, tracks were accepted only in the range $|\eta| < 0.8$ (i.e. well within the TPC acceptance) and with $p_T > 0.15$ GeV/ c . In order to reduce secondary particles, tracks were required to have at least one hit in one of the two innermost tracking detectors (SPD) and to have a DCA to the primary vertex less than 2 cm along the beam direction. The DCA in the transverse plane was required to be smaller than $7 \sigma_{DCA}(p_T)$, where $\sigma_{DCA}(p_T) = (0.0026 + 0.0050 \text{ GeV}/c \cdot p_T^{-1})$ cm.

4.2 Particle identification

Identification of pions and kaons is performed using the measurements of the TPC and the TOF. For the TPC, the particle is identified based on the energy it deposits in the drift gas, compared with the expected value computed using a parameterized Bethe-Bloch function [24, 25]. Figure 1

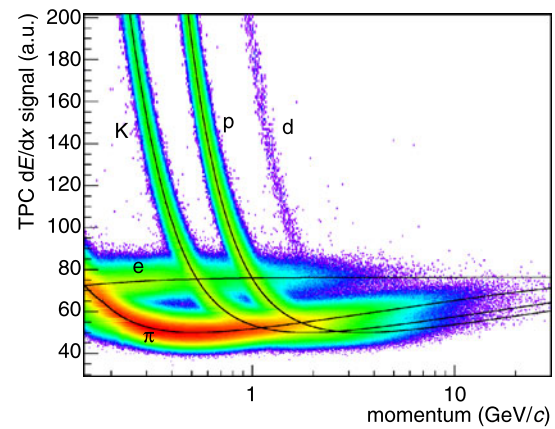


Fig. 1 Specific ionization energy loss dE/dx vs. momentum for tracks measured with the ALICE TPC. The *solid lines* are parametrizations of the Bethe-Bloch function [24] (Colour figure online)

shows the TPC signal versus track momentum computed at the point the particle enters the detector, and the curves represent the Bethe-Bloch functions for each mass hypothesis. The TPC calibration parameters have mostly been determined and tested via the analysis of cosmic rays; the chamber gain has been measured using the decay of radioactive ^{83}Kr gas released into the TPC volume [18].

A truncated-mean procedure is used to determine dE/dx , with only 60 % of the points kept. The dE/dx resolution σ_{TPC} is about 5 % for tracks with 159 clusters and about 6.5 % when averaged over all reconstructed tracks. The relevant value of σ_{TPC} is estimated for each track taking into account the actual number of clusters used [18].

The TPC dE/dx measurement allows pions to be separated from kaons for momenta up to $p \sim 0.7$ GeV/ c , while the proton/antiproton band starts to overlap with the pion/kaon band at $p \approx 1$ GeV/ c . As can be observed in Fig. 1, the electron/positron dE/dx band crosses the other bands at various momenta. This contamination in identified pions and kaons can be drastically reduced using information from the TOF.

Particles are identified in the TPC via the difference between the measured energy loss and the value expected for different mass hypotheses. The cut on this difference, normalized to the resolution σ_{TPC} , is optimized for each analysis and depends in general on the signal-to-background ratio and on the transverse momentum.

Figure 2 shows the correlation between particle momentum and their velocity $\beta = L/ct$, where L is the total integrated path length and t is the time of flight measured by the TOF detector. For the analyses described in this paper the start time of the collision is estimated using the particle arrival times at the TOF or the averaged collision time observed in the fill. The bands corresponding to pions, kaons, protons and deuterons are clearly visible.

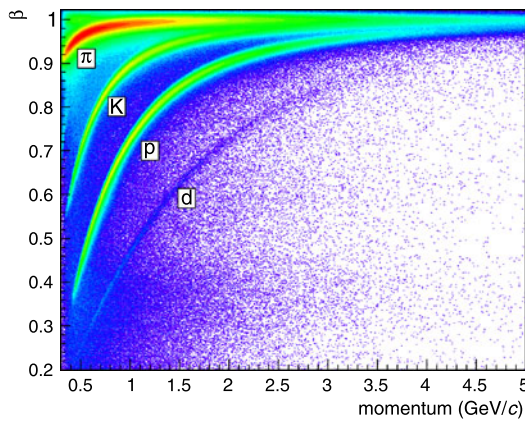


Fig. 2 Velocity β of particles measured by TOF vs. momentum (Colour figure online)

Particles are identified in the TOF by comparing the measured time of flight to the expected time for a given particle species. The cut is expressed in units of the estimated resolution σ_{TOF} for each track, which has a mean value of 160 ps. The TOF allows pions and kaons to be unambiguously identified up to $p \sim 1.5$ GeV/c. The two mesons can be distinguished from (anti)protons up to $p \sim 2.5$ GeV/c.

Considering the high multiplicities reached in pp collisions at LHC energies, good particle identification is important to reduce combinatorial background as well as correlated background from misidentified resonance decays. The ϕ analysis requires only primary kaons to be selected and cuts were kept loose in order to maximize the efficiency. The cut for particle identification in the TPC was set to $3\sigma_{\text{TPC}}$ ($5\sigma_{\text{TPC}}$) for tracks with p larger (smaller) than 0.35 GeV/c. When a TOF signal is present, a particle identification cut of $3\sigma_{\text{TOF}}$ is also applied. For the K^* analysis, both pions and kaons are identified. Two different strategies were followed. For tracks with TOF signals, a TPC dE/dx cut of $5\sigma_{\text{TPC}}$ was applied and a TOF cut of $3\sigma_{\text{TOF}}$ ($2\sigma_{\text{TOF}}$) was applied for tracks with momenta below (above) 1.5 GeV/c. For tracks without a TOF signal, $5\sigma_{\text{TPC}}$, $3\sigma_{\text{TPC}}$, and $2\sigma_{\text{TPC}}$ cuts were used for $p < 0.35$ GeV/c, $0.35 < p < 0.5$ GeV/c, and $p > 0.5$ GeV/c, respectively; the kaon momentum was required to be below 0.7 GeV/c. This more restrictive cut on kaons was used to reduce the correlated background originating from ρ decays in which a pion is misidentified.

4.3 Raw yield extraction and background estimation

The uncorrelated background was estimated using two different techniques: like-sign and event mixing. In the like-sign method invariant mass distributions of like-sign $K\pi$ or KK combinations (for K^* and ϕ , respectively) from the same event were constructed. In the event mixing method the shape of the uncorrelated background was estimated from the invariant mass distribution of unlike-sign $K\pi$ or

KK combinations from different events. To avoid mismatch due to different acceptances and to assure a similar event structure, tracks from events with similar vertex positions z ($\Delta z < 1$ cm) and track multiplicities n ($\Delta n < 10$) were mixed. To reduce statistical uncertainties each event was mixed with 10 other events. The mixed-event distribution was then normalized in the mass region $1.08 < M < 1.2$ ($1.04 < M < 1.07$) GeV/ c^2 for K^* (ϕ), and subtracted in each p_T bin. The uncertainty in the normalization was estimated by varying the normalization region and is included in the quoted systematic uncertainty for signal extraction. After background subtraction a residual background remains. This is due in part to an imperfect description of the combinatorial background but mainly caused by a real correlated background. The latter can arise from correlated πK or KK pairs or from misidentified particle decays (for example K^{*0} for ϕ , or ϕ and ρ for K^* , or from underlying jet event structure).

The total p_T -integrated number of reconstructed mesons after background subtraction was about 1.8×10^6 for the K^* and 2.3×10^5 for the ϕ . For the K^* the signal-to-background ratio varied from 0.08 at $p_T = 0.05$ GeV/c to 0.2 at $p_T = 5.5$ GeV/c. The significance ($S/\sqrt{S+B}$) was about 34 in the p_T bins at both 0.05 and 5.5 GeV/c and reached a maximum of about 127 at 1 GeV/c. For the ϕ the signal-to-background ratio varied from 2.8 to 1.6 between $p_T = 0.45$ and $p_T = 5.5$ GeV/c, with a minimum of 0.5 at 1.6 GeV/c; the significance was about 30 in the p_T bins at both 0.45 and 5.5 GeV/c with a maximum of 90 at 1 GeV/c.

The raw yield of $K^*(892)^0$ and its antiparticle was extracted in 22 p_T bins between 0 and 6 GeV/c in the rapidity range $|y| < 0.5$. The combinatorial background was subtracted using like-sign $\pi^\pm K^\pm$ pairs. The mass distribution $M(\pi^\pm, K^\mp)$ (see Fig. 3 for two p_T bins) was fitted with a relativistic Breit-Wigner function multiplied by a Boltzmann factor [3] and added to a polynomial residual background. The width was found to be compatible, within uncertainties, with the natural value. At low p_T the fitted mass values were found to be slightly lower (by about ≈ 5 MeV/ c^2) than the natural value, which is attributed to imperfections in corrections for the energy loss in the detector material. To extract the yield the distribution of $M(\pi^\pm, K^\mp)$ was then fitted with a (non-relativistic) Breit-Wigner function with the width fixed to its natural value ($\Gamma = 48.7 \pm 0.8$ [26]) and a background function:

$$\frac{dN}{dM} = \frac{1}{2\pi} \frac{A\Gamma}{(M - M_0)^2 + \Gamma^2/4} + B(M) \quad (1)$$

where A is the area under the peak corresponding to the number of K^* mesons, Γ is the full width at half maximum of the peak, and M_0 is the resonance mass. The residual background $B(M)$, after like-sign subtraction, was parametrized by a polynomial (dashed line in Fig. 3).

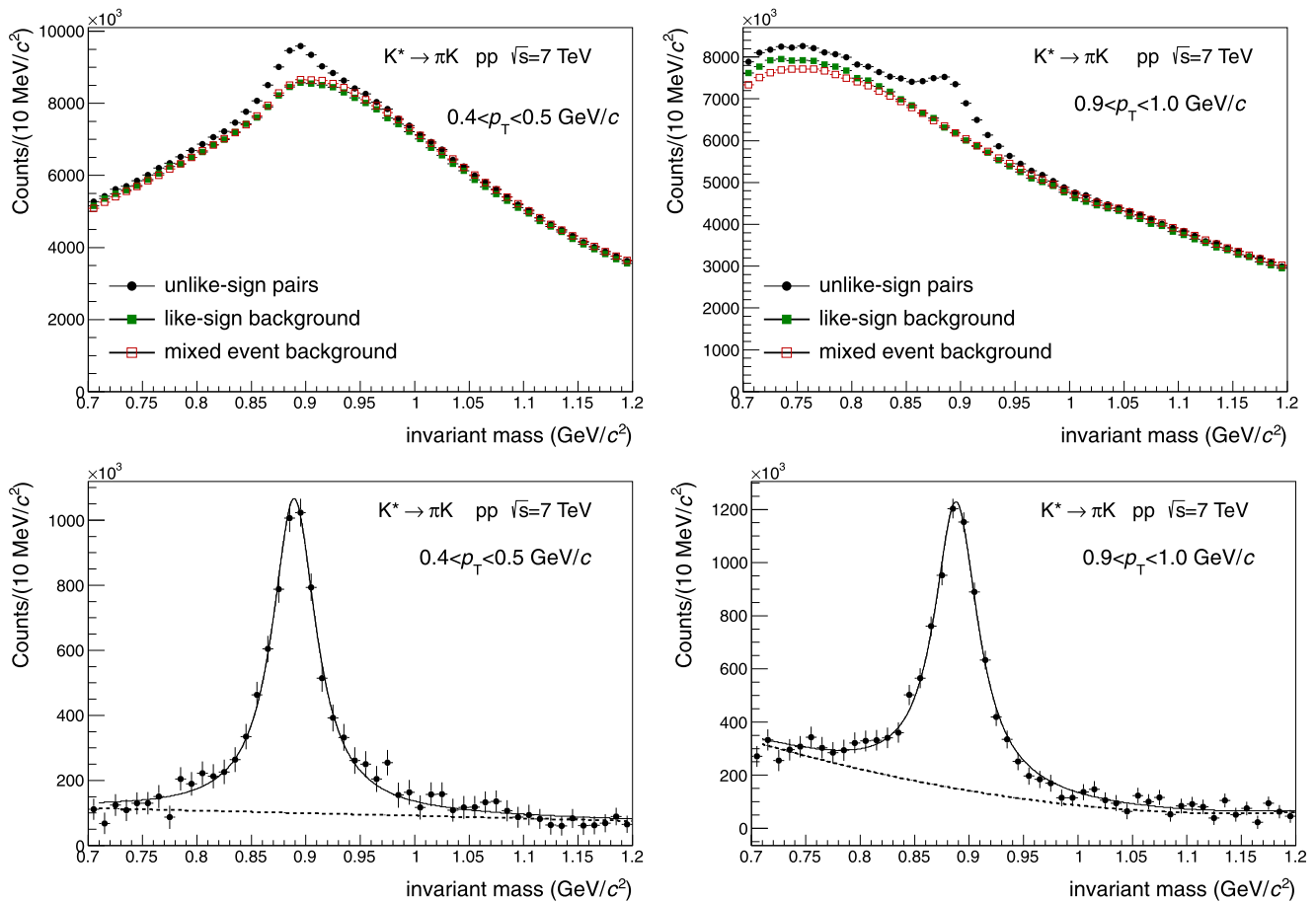


Fig. 3 (Upper panel) The $\pi^{\pm}K^{\mp}$ invariant mass distribution in $|y| < 0.5$ for the bin $0.4 < p_T < 0.5$ GeV/c (left) and $0.9 < p_T < 1.0$ GeV/c (right), in pp collisions at 7 TeV. The background shape estimated using unlike-sign pairs from different events (event mixing) and like-sign pairs from the same event are shown as open red squares and full

green squares, respectively. (Lower panel) The $\pi^{\pm}K^{\mp}$ invariant mass distribution after like-sign background subtraction for $0.4 < p_T < 0.5$ GeV/c (left) and $0.9 < p_T < 1.0$ GeV/c (right). The solid curve is the result of the fit by Eq. (1), the dashed line describes the residual background (Colour figure online)

For the ϕ meson, the raw yield was extracted from the K^+K^- invariant mass distributions in 26 p_T bins between 0.4 and 6 GeV/c. The combinatorial background was subtracted using a polynomial fit (first or second order), like-sign pairs, or unlike-sign pairs from mixed events (Fig. 4 for two p_T bins). Since the invariant mass resolution of the ϕ peak is of the same order of magnitude as the natural ϕ width (~ 1 MeV/ c^2 vs. 4.26 MeV/ c^2), the fit is performed, after background subtraction, using a Voigtian function (convolution of Breit-Wigner function and Gaussian) superimposed on a polynomial to describe the residual background:

$$\frac{dN}{dM} = A \int \frac{\Gamma/2\pi}{(M - M')^2 + \Gamma^2/4} \frac{e^{-(M' - M_0)^2/2\sigma^2}}{\sqrt{2\pi}\sigma} dM' + B(M) \quad (2)$$

where σ represents the mass resolution and the other parameters have the same meaning as in Eq. (1). The background $B(M)$ is represented in the lower panels of Fig. 4 by

a dashed line. The width Γ is fixed to its nominal value [26] while σ is a free parameter. The fitted mass values were found to be compatible, within uncertainties, with the known mass [26], with the exception of the low p_T range 0.4 – 0.7 GeV/c where a fitted value lower than the natural one (by $< 0.1\%$) was observed. The raw yields extracted using the three different methods to estimate the combinatorial background (analytic function, like-sign and mixed-event method) were found to be compatible within a few percent; therefore the mean value of all three methods was taken in each p_T bin.

4.4 Efficiency corrections

In order to extract the meson yields, the raw counts (N^{RAW}) were corrected for the decay branching ratio [26] and for losses due to pion/kaon in-flight decays, geometrical acceptance, and detector efficiency ($N^{\text{COR}} = N^{\text{RAW}}/(A \times \epsilon)\text{BR}$, where BR indicates the decay branching ratio). The product

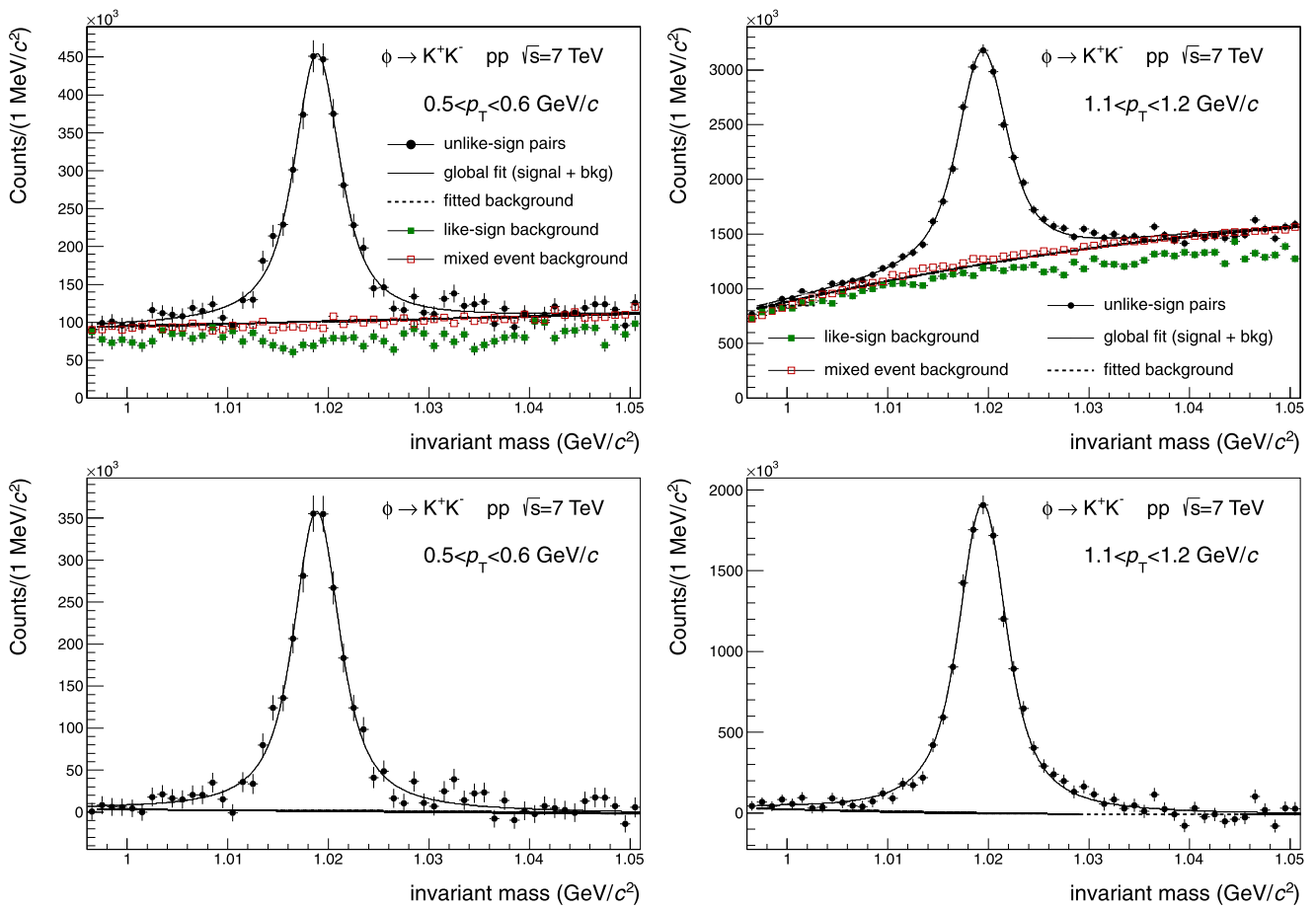


Fig. 4 (Upper panel) The K^+K^- invariant mass distribution in $|y| < 0.5$, for the bin $0.5 < p_T < 0.6$ GeV/c (left) and $1.1 < p_T < 1.2$ GeV/c (right) in pp collisions at 7 TeV. The solid curve is the fit result (Eq. (2)), while the dashed line describes the background. The background shape estimated using unlike-sign pairs from different events (event mixing) or like-sign pairs from the same event

are shown as open red squares and full green squares, respectively. (Lower panel) The K^+K^- invariant mass distribution after mixed-event background subtraction for $0.5 < p_T < 0.6$ GeV/c (left) and $1.1 < p_T < 1.2$ GeV/c (right). The solid curve is the fit result (Eq. (2)), while the dashed line describes the residual background (Colour figure online)

of acceptance and efficiency ($A \times \epsilon$) was determined for K^* and ϕ from Monte Carlo simulations with the PYTHIA 6.4 event generator (tune Perugia 0 [15]) and a GEANT3-based simulation of the ALICE detector response. About 60 M Monte Carlo events, with the same vertex distribution as the measured events, were analyzed in exactly the same way as the data. The dependence on the event generator was estimated to be below 1 % by comparing PYTHIA and PHOJET simulated events. The $A \times \epsilon$ was determined from the Monte Carlo simulations as the ratio of the number of reconstructed resonances to the number of those generated, differentially as a function of rapidity and transverse momentum. The transverse momentum dependence is shown in Fig. 5 for K^* and ϕ mesons. The decrease in $A \times \epsilon$ at low p_T is due to the minimum p_T requirement for reconstructed tracks, while the different behaviour for ϕ and K^* is due to the different Q -value of their decay (31.1 MeV for ϕ and 262.7 MeV for K^*).

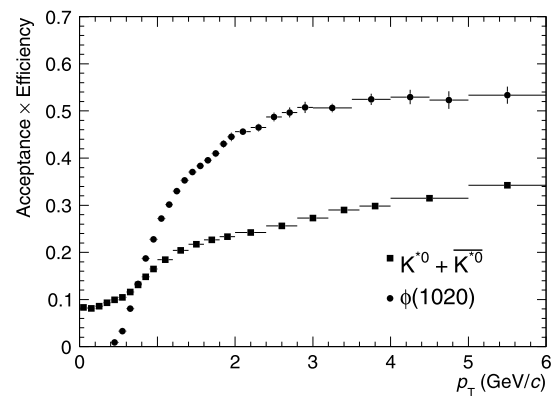


Fig. 5 The product of acceptance and efficiency of K^* and ϕ detection as a function of p_T in $|y| < 0.5$. Statistical uncertainties are reported. Contributions to the point-to-point systematic uncertainties are listed in Table 1

Finally, corrections for the trigger efficiency ($\epsilon_{\text{trigger}}$) and the required primary vertex range (ϵ_{vert}) were applied in order to obtain the absolute resonance yields per inelastic collision:

$$\frac{d^2N}{dydp_T} = \frac{N^{\text{cor}}(p_T)}{\Delta y \Delta p_T} \times \frac{1}{\epsilon_{\text{vert}}} \times \frac{\epsilon_{\text{trigger}}}{N_{\text{MB}}} \quad (3)$$

here N^{cor} and N_{MB} are the number of reconstructed K^* or ϕ and the total number of minimum bias triggers, respectively. The value of the trigger selection efficiency for inelastic collisions $\epsilon_{\text{trigger}}$ is reported in Sect. 3. The loss of resonances due to the trigger selection, estimated by Monte Carlo, is negligible, less than 0.2 %. The ϵ_{vert} correction factor accounts for resonance losses (≈ 1 %) due to the requirement to have a vertex in the range of ± 10 cm.

4.5 Estimation of the systematic uncertainties

The minimum and maximum values of the major contributions to the point-to-point systematic uncertainties are listed in Table 1. The uncertainty due to the raw yield extraction method was found to be ± 2 –28 % (2–10 %) for K^* (ϕ). It was estimated by changing the mass range considered for the fit and the order of the polynomial for the residual background function (from first through third (second) order for K^* (ϕ)). Finally, variations in the yield due to the method used to estimate the combinatorial background (like-sign and event-mixing method and also analytic function for ϕ) were incorporated into the systematic uncertainties. For the K^* a relativistic Breit-Wigner function was used to fit the mass peak in addition to the non-relativistic version. In the case of the K^* a rather large systematic uncertainty was estimated for the higher p_T bins, due to the presence of a correlated background.

The uncertainty introduced by the tracking and PID efficiency was estimated to be ± 8 % (8 %) and ± 1 –6 % (1.5 %) respectively in the case of K^* (ϕ) by varying the kinematical and PID cuts on the daughter tracks. An additional ± 1 –4 % uncertainty was added for the K^* due to differences observed in the TOF matching efficiency between data and Monte Carlo. The uncertainty on the yield contained in the extrapolated part of the ϕ spectrum was estimated to be ± 20 % using different fit functions. The normalization to the

number of inelastic collisions leads to a +6.2 % and -3 % uncertainty in the yield of the measured particles. The resulting overall systematic uncertainty is $^{+10}_{-9}$ % ($^{+12.5}_{-11}$ %) for the K^* (ϕ) yield dN/dy and ± 2 % (3 %) for the average transverse momentum $\langle p_T \rangle$.

5 Results and discussion

5.1 p_T spectra and integrated yield

Figure 6 presents the corrected p_T spectra for the two resonances. The statistical and point-to-point systematic uncertainties added in quadrature are shown. The spectra are fitted with a Lévy-Tsallis function [27, 28]

$$\frac{d^2N}{dydp_T} = \frac{(n-1)(n-2)}{nT[nT+m(n-2)]} \times \frac{dN}{dy} \times p_T \times \left(1 + \frac{m_T - m}{nT}\right)^{-n} \quad (4)$$

where $m_T = \sqrt{m^2 + p_T^2}$. This function describes both the exponential shape of the spectrum at low p_T and the power-law distribution at large p_T , quantified by the inverse slope parameter T and the exponent parameter n , respectively. The extracted parameter values are listed in Table 2 and the fits are shown in Fig. 6. The χ^2/ndf values are smaller than unity because the point-to-point systematic uncertainties, which are included in the fit, could be correlated.

The extracted n values are similar to those quoted by the STAR experiment at RHIC for the ϕ measured in pp collisions at 200 GeV ($n = 8.3 \pm 1.2$) [5]. In contrast, the slope parameters are significantly higher than the values obtained at RHIC, $T = 202 \pm 14 \pm 11$ MeV for ϕ , and $T = 223 \pm 8 \pm 9$ MeV for K^* [3] (the latter was obtained

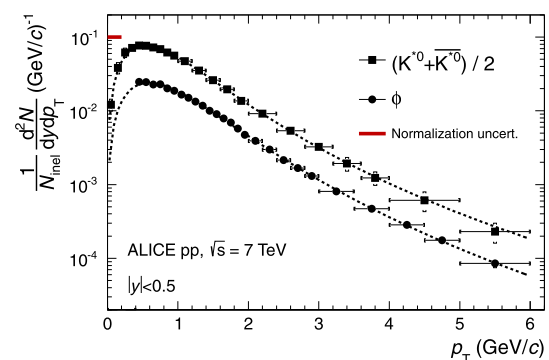


Fig. 6 Transverse momentum spectra for K^* and $\phi(1020)$ in pp collisions at $\sqrt{s} = 7$ TeV. The statistical and systematic uncertainties are added in quadrature and the uncertainty due to normalization [21] is shown separately. The statistical uncertainty is smaller than the symbol size. Each spectrum is fitted with a Lévy-Tsallis function (dashed line)

Table 1 Summary of the systematic point-to-point uncertainties in the K^* and ϕ yield

Source of uncertainty	K^*	ϕ
Signal extraction	± 2 –28 %	± 2 –10 %
Tracking efficiency	± 8 %	± 8 %
PID efficiency	± 1 –6 %	± 1.5 %
TOF matching efficiency	± 1 –4 %	–

Table 2 Parameters extracted from the Lévy-Tsallis (4) fits to the K^* and ϕ transverse momentum spectra in 7 TeV pp collisions, including point-to-point systematic uncertainties. The first uncertainty is statistical and the second is systematic

Particles	χ^2/ndf	T (MeV)	n
K^*	2.0/19	$254 \pm 2 \pm 18$	$6.2 \pm 0.07 \pm 0.8$
ϕ	2.8/23	$272 \pm 4 \pm 11$	$6.7 \pm 0.20 \pm 0.4$

Table 3 K^* and ϕ yield and $\langle p_T \rangle$ estimated in the range 0–6 GeV/c in inelastic pp collisions at $\sqrt{s} = 7$ TeV. The systematic uncertainties of dN/dy and $\langle p_T \rangle$ include contributions from the choice of spectrum fit function for extrapolation, the absolute normalization, and the point-to-point uncertainties listed in Table 1

Particles	measured p_T (GeV/c)	dN/dy	$\langle p_T \rangle$ (GeV/c)
K^*	[0.0–6.0]	$0.097 \pm 0.0004^{+0.010}_{-0.009}$	$1.01 \pm 0.003 \pm 0.02$
ϕ	[0.4–6.0]	$0.032 \pm 0.0004^{+0.004}_{-0.0035}$	$1.07 \pm 0.005 \pm 0.03$

by an exponential fit and can therefore not be directly compared).

The total yields dN/dy and the mean transverse momentum $\langle p_T \rangle$, including statistical and systematic uncertainties, are listed in Table 3. The values of dN/dy were obtained by integrating the spectra in the measured range and extrapolating to zero p_T with the fitted Lévy-Tsallis function. The contribution of the low- p_T extrapolation is negligible for the K^* and about $15 \pm 3\%$ for the ϕ . The mean transverse momentum was estimated in the range $0 < p_T < 6$ GeV/c using the Lévy-Tsallis function. However, similar values are obtained when calculating the mean from the measured data points, using the fit only to extrapolate into the unmeasured p_T regions. In addition to the point to point systematic uncertainties previously described, an exponential fit was also used to estimate the systematic uncertainty in $\langle p_T \rangle$ due to a different choice of fit function. Compared to pp collisions at 200 GeV [3, 5, 29], the mean p_T rises by about 30 % (Fig. 7) and the yield per inelastic collision increases by about a factor of two, which is similar to the overall increase of charged particle multiplicity [30, 31].

The ϕ yield, measured via the leptonic decay channel in the ALICE muon spectrometer in $2.5 < y < 4$, $1 < p_T < 5$ GeV/c [32], has a similar momentum distribution, but is lower by about 30 % at forward rapidity. The ϕ yield is expected to vary by 20 %–50 % between forward ($2.5 < y < 4$) and mid-central ($-0.5 < y < 0.5$) rapidities, based on analysis of different PYTHIA tunes described in Sect. 5.2. In particular, the lower value is predicted from the D6T PYTHIA tune [36, 37], which reproduces rather well the ϕ spectrum at forward rapidity [32] and the low p_T part of the ϕ spectrum at mid-rapidity (see Fig. 9 described in Sect. 5.2).

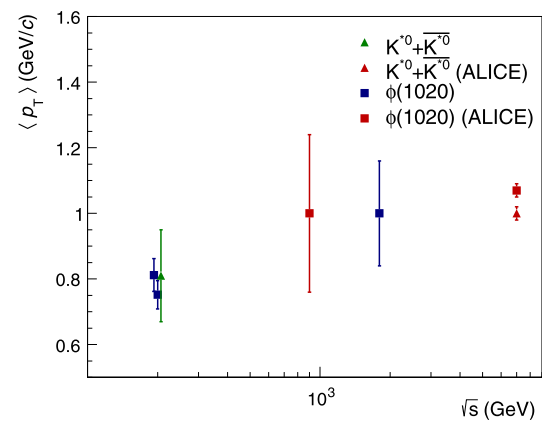


Fig. 7 Energy dependence of $\langle p_T \rangle$ for K^* (triangles) and ϕ (squares) in pp collisions. The points at lower energies are from STAR and PHENIX ($\sqrt{s} = 200$ GeV) [3, 5, 29], ALICE ($\sqrt{s} = 0.9$ TeV) [33] and E735 ($\sqrt{s} = 1.8$ TeV) [34]. The STAR data have been slightly displaced to separate the K^* and the ϕ . The data point at 1.8 TeV represents the mean of the two values quoted from the E735 collaboration in [34], obtained from two different fit functions of the ϕ p_T distribution

5.2 Comparisons to models

Multiparticle production, which is predominantly a soft, non-perturbative process, is usually modelled by QCD inspired Monte Carlo event generators like PHOJET [9, 10] and PYTHIA [11]. In both models, hadronization is simulated using the Lund string fragmentation model [35]. Different PYTHIA tunes were obtained by adjusting the model parameters to reproduce existing data. The D6T tune [36, 37], which uses the CTEQ6L parton distribution function (with a corresponding larger production of strange particles), was obtained by fitting CDF Run 2 data. The ATLAS-CSC [38] tune was adjusted to minimum bias data from the UA5, E735, and CDF experiments for energies ranging from 0.2 to 1.8 TeV. The latest PYTHIA tune, Perugia 2011 [15], takes into account first results from the LHC, in particular minimum-bias and underlying event data at 0.9 and 7 TeV. Strange baryon production was increased in this tune leading to a larger Λ/K ratio with respect to the Perugia 0 tune.

The transverse momentum spectra of K^* and ϕ are compared to PHOJET and various PYTHIA tunes in Figs. 8 and 9. For PYTHIA, tunes D6T (109), ATLAS-CSC (306), Perugia 0 (320) and Perugia 2011 (350) were used. The best agreement is found for the PYTHIA Perugia 2011 tune, which reproduces both the K^* spectrum and the high p_T part ($p_T > 3$ GeV/c) of the ϕ spectrum rather well. PHOJET and ATLAS-CSC very significantly overestimate the low momentum part ($p_T < 1$ GeV/c) of the transverse momentum distribution but reproduce the high momentum distribution of both mesons well. The PYTHIA D6T tune gives the best description at low p_T , but deviates from the data at $p_T > 2$ GeV/c. Finally, the PYTHIA Perugia 0 tune underestimates the meson yield for p_T larger than 0.5 GeV/c.

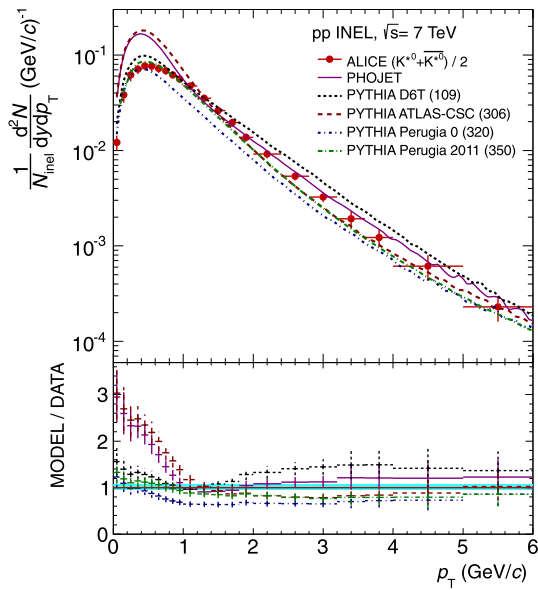


Fig. 8 Comparison of the K^* p_T spectra in inelastic pp collisions with PHOJET and PYTHIA tunes D6T (109), ATLAS-CSC (306), Perugia 0 (320), and Perugia 2011 (350) (Colour figure online)

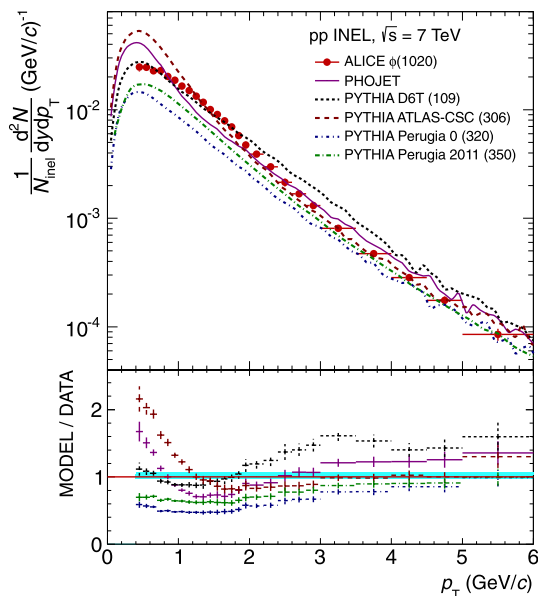


Fig. 9 Comparison of the $\phi(1020)$ p_T spectra in inelastic pp collisions with PHOJET and PYTHIA tunes D6T (109), ATLAS-CSC (306), Perugia 0 (320), and Perugia 2011 (350) (Colour figure online)

Similar comparisons for the mid- and forward-rapidity ϕ spectrum in pp collisions at $\sqrt{s} = 0.9$ TeV [33] and 7 TeV [32], respectively, show that the ϕ spectrum is rather well reproduced by the ATLAS-CSC and D6T tunes, while the Perugia 0 and 2011 tunes underestimate the data. Moreover the PYTHIA tunes generally underestimate strange meson and hyperon production in 7 TeV pp collisions [13, 39],

while the Perugia 2011 tune gives a good description of kaon production in pp collisions at 7 TeV [12].

5.3 Particle ratios

The measurement of particle production and particle ratios in pp collisions is important as a baseline for comparison with heavy ion reactions. In heavy ion collisions, the yields for stable and long-lived hadrons reflect the thermodynamic conditions (temperature, chemical potentials) at freeze-out, whereas the yield for short-lived resonances can be modified by final state interactions inside the hot and dense reaction zone [40, 41]. Particularly interesting is the comparison of ϕ and K^* production, considering the different lifetimes (about a factor 10) of the two resonances.

Using different particle ratios (like K/π or ϕ/K^*) measured in elementary collisions, values ranging from 0.1 to 0.4 [1, 2, 43–45] were previously obtained for the strange quark suppression factor $\lambda_s = 2s\bar{s}/(u\bar{u} + d\bar{d})$, which represents the probability to produce strange quark pairs relative to light quarks [42]. In pp reactions, particle abundances have been successfully described by statistical-thermal models. Now, using measured identified particle yields, an energy-independent value of 0.2 for λ_s has been extracted in e^+e^- , pp, and $p\bar{p}$ collisions at $\sqrt{s} < 1$ TeV [42, 46].

Using the ϕ and K^* yields presented in this paper and stable particle results measured by ALICE at the same energy [12], we find the following values for particle ratios in pp collisions at 7 TeV: $K^*/K^- = 0.35 \pm 0.001$ (stat.) ± 0.04 (syst.), $\phi/K^* = 0.33 \pm 0.004$ (stat.) ± 0.05 (syst.), $\phi/K^- = 0.11 \pm 0.001$ (stat.) ± 0.02 (syst.), $\phi/\pi^- = 0.014 \pm 0.0002$ (stat.) ± 0.002 (syst.). Due to the fact that the same data were analyzed to extract both resonance and non-resonance (π , K) yields, the uncertainties due to the absolute normalization cancel and are therefore not included in the systematic uncertainties of the ratios. These ratios are shown in Figs. 10 and 11, together with the results obtained at lower incident energies in pp, e^+e^- , and A–A collisions.

The K^*/K^- , ϕ/K^- , and ϕ/K^* ratios are essentially independent of energy and also independent of the collision system, with the exception of K^*/K and ϕ/K^* at RHIC [5, 51–53], where these ratios in nuclear collisions are respectively lower and higher than in pp. On the contrary, the ϕ/π ratio increases with energy both in heavy ion and in pp collisions up to at least 200 GeV. However, in heavy ion collisions the value obtained by the PHENIX experiment [4], about 40 % lower than the STAR result [5] at the same collision energy, seems indicate a saturation of this ratio at the RHIC energies. In pp collisions we observe a saturation of the ϕ/π ratio, with no significant change over the LHC energy range between 1 and 7 TeV.

In microscopic models where soft particle production is governed by string fragmentation, strange hadron yields are

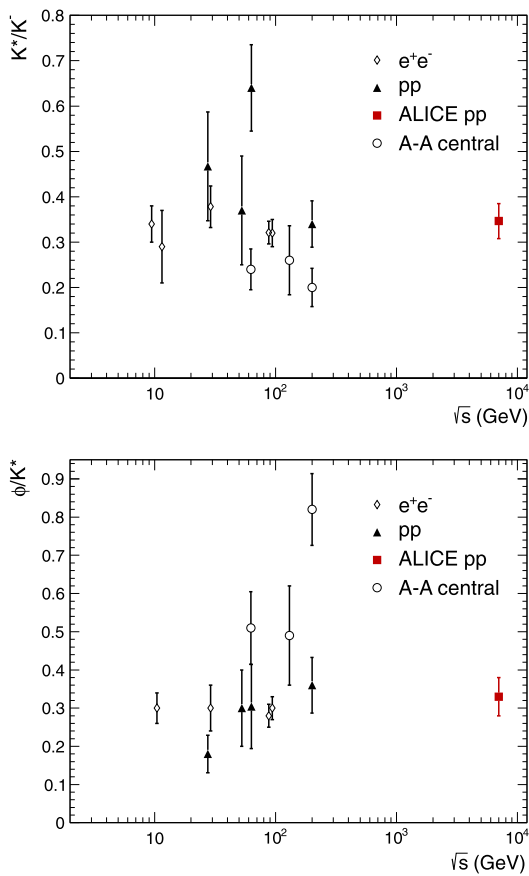


Fig. 10 Energy dependence of the K^*/K^- (upper panel) and ϕ/K^* (lower panel) ratio in e^+e^- (diamonds) [2, 43, 44, 48, 62], and pp (triangles) [1, 3, 5, 49–51] collisions. Red squares represent the data from the ALICE experiment for 7 TeV pp collisions, K^- yields are from [12]. Open circles represent the same ratios in central nucleus-nucleus collisions from [3, 5, 51–53]. Some points have been displaced horizontally for better visibility. Ratios are calculated from yields at mid-rapidity or in full space (Colour figure online)

predicted to depend on the string tension [8]. Multi-strange baryons, and in particular the ratio Ω/ϕ , are expected to be very sensitive to this effect [14]. The ϕ yield is compared to the $\Omega^- + \bar{\Omega}^+$ data measured by ALICE at the same incident energy [13] in Fig. 12 as a function of transverse momentum. The full line represents the PYTHIA model (Perugia 2011 tune), which is a factor 1.5–5 below the data. While this tune describes the ϕ spectrum reasonably well above 2–3 GeV/c, it underpredicts multistrange baryon yields by a large factor [13]. The dashed line, which is very close to the data, represents the prediction of a model with increased string tension, the HIJING/B \bar{B} v2.0 model with a Strong Colour Field (SCF), for pp collisions at 5.5 TeV [14]. This is a model that combines multiple minijet production via perturbative QCD with soft longitudinal string excitation and hadronization. In this case the SCF effects are modeled by varying the effective string tensions that controls the $q\bar{q}$ and $qq\bar{q}q$ pair creation rates and the strangeness sup-

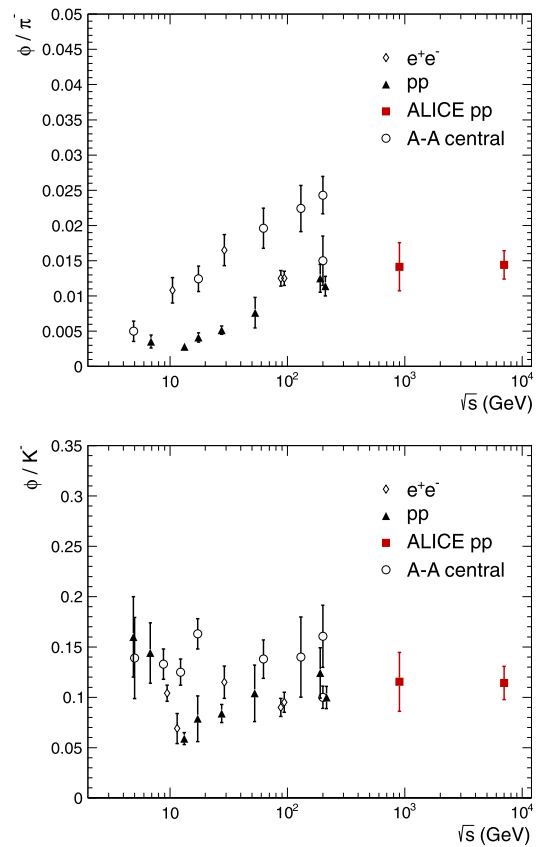


Fig. 11 Energy dependence of the ϕ/π^- (upper panel) and ϕ/K^- ratio (bottom panel) in nuclear (open circles) [4, 5, 52, 54–57], e^+e^- (diamonds) [2, 43, 44, 48, 62], and pp (triangles) [1, 3, 5, 29, 47, 49, 54–56, 59] collisions. Other π^- and K^- yields are from [58–61]. Red squares represent the ALICE data at 0.9 and 7 TeV. The pion and kaon yields at 7 TeV are from [12]. The ϕ , π^- , and K^- yields at 0.9 TeV are from [25, 33]. Some points have been displaced horizontally for better visibility. Ratios are calculated from yields at mid-rapidity or in full space, except the data at $\sqrt{s} = 4.87$ GeV [54] (Colour figure online)

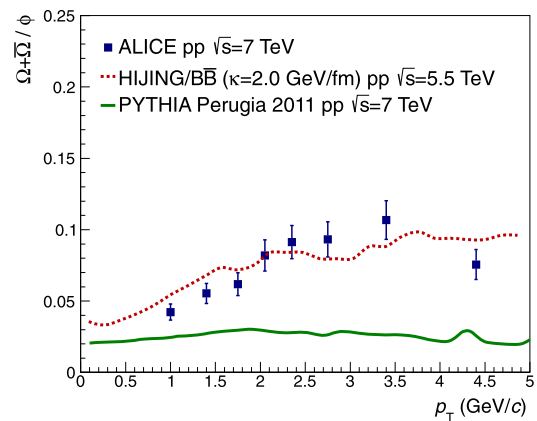


Fig. 12 $(\Omega + \bar{\Omega})/\phi$ ratio as a function of transverse momentum for pp collisions at $\sqrt{s} = 7$ TeV. Ω data are from [13]. The dashed line represents the prediction of HIJING/B \bar{B} v2.0 model with a SCF for pp collisions at $\sqrt{s} = 5.5$ TeV with a string tension of 2 GeV/fm [14]. The same calculation at 7 TeV yields a $\sim 10\%$ higher ratio [64]. The full line represents the prediction of the PYTHIA Perugia 2011 tune [15] for pp collisions at $\sqrt{s} = 7$ TeV (Colour figure online)

pression factor. The value of string tension used in this calculation is $\kappa = 2$ GeV/fm, equal to the value used to fit the high baryon/meson ratio at $\sqrt{s} = 1.8$ TeV reported by the CDF collaboration [63]. The same calculation at 7 TeV yields a ~ 10 % higher ratio [64]. Higher values of the string tension (~ 3 GeV/fm) also successfully reproduce also the $(\Omega + \bar{\Omega})/\phi$ ratio in Au–Au collisions at $\sqrt{s} = 200$ GeV [14], but overestimate the $(\Lambda + \bar{\Lambda})/K_S^0$ at 7 TeV [8].

6 Conclusion

Yields and spectra of $K^*(892)^0$ and $\phi(1020)$ mesons were measured for inelastic pp collisions at $\sqrt{s} = 7$ TeV by the ALICE collaboration at the LHC. The transverse momentum spectra are well described by the Lévy–Tsallis function. The yields for both mesons increase by about a factor of two from 200 GeV centre-of-mass energy, and the average p_T by about 30 %.

The K^*/K and ϕ/K^* ratios (and consequently the ϕ/K ratio) are found to be independent of energy up to 7 TeV. Also the ϕ/π ratio, which increases in both pp and A–A collisions up to at least RHIC energies, saturates and becomes independent of energy above 200 GeV.

The data have been compared to a number of PYTHIA tunes and the PHOJET event generator. None of them gives a fully satisfactory description of the data. The latest PYTHIA version (Perugia 2011) comes closest, while still underpredicting the ϕ meson p_T spectrum below 3 GeV/ c by up to a factor of two.

The $(\Omega^- + \bar{\Omega}^+)/\phi$ ratio is not reproduced by PYTHIA Perugia 2011, but is in good agreement with the HIJING/ $\bar{B}\bar{B}$ v2.0 model with SCF, which enhances multi-strange baryon production by increasing the string tension parameter.

Acknowledgements The ALICE collaboration would like to thank all its engineers and technicians for their invaluable contributions to the construction of the experiment and the CERN accelerator teams for the outstanding performance of the LHC complex.

The ALICE collaboration acknowledges the following funding agencies for their support in building and running the ALICE detector: Calouste Gulbenkian Foundation from Lisbon and Swiss Fonds Kidagan, Armenia; Conselho Nacional de Desenvolvimento Científico e Tecnológico (CNPq), Financiadora de Estudos e Projetos (FINEP), Fundação de Amparo à Pesquisa do Estado de São Paulo (FAPESP); National Natural Science Foundation of China (NSFC), the Chinese Ministry of Education (CMOE) and the Ministry of Science and Technology of China (MSTC); Ministry of Education and Youth of the Czech Republic; Danish Natural Science Research Council, the Carlsberg Foundation and the Danish National Research Foundation; The European Research Council under the European Community's Seventh Framework Programme; Helsinki Institute of Physics and the Academy of Finland; French CNRS-IN2P3, the 'Region Pays de Loire', 'Region Alsace', 'Region Auvergne' and CEA, France; German BMBF and the Helmholtz Association; General Secretariat for Research and Technology, Ministry of Development, Greece; Hungarian OTKA and

National Office for Research and Technology (NKTH); Department of Atomic Energy and Department of Science and Technology of the Government of India; Istituto Nazionale di Fisica Nucleare (INFN) of Italy; MEXT Grant-in-Aid for Specially Promoted Research, Japan; Joint Institute for Nuclear Research, Dubna; National Research Foundation of Korea (NRF); CONACYT, DGAPA, México, ALFA-EC and the HELEN Program (High-Energy physics Latin-American–European Network); Stichting voor Fundamenteel Onderzoek der Materie (FOM) and the Nederlandse Organisatie voor Wetenschappelijk Onderzoek (NWO), Netherlands; Research Council of Norway (NFR); Polish Ministry of Science and Higher Education; National Authority for Scientific Research—NASR (Autoritatea Națională pentru Cercetare Științifică—ANCS); Federal Agency of Science of the Ministry of Education and Science of Russian Federation, International Science and Technology Center, Russian Academy of Sciences, Russian Federal Agency of Atomic Energy, Russian Federal Agency for Science and Innovations and CERN-INTAS; Ministry of Education of Slovakia; Department of Science and Technology, South Africa; CIEMAT, EELA, Ministerio de Educación y Ciencia of Spain, Xunta de Galicia (Consellería de Educación), CEADEN, Cubaenergía, Cuba, and IAEA (International Atomic Energy Agency); Swedish Research Council (VR) and Knut & Alice Wallenberg Foundation (KAW); Ukraine Ministry of Education and Science; United Kingdom Science and Technology Facilities Council (STFC); The United States Department of Energy, the United States National Science Foundation, the State of Texas, and the State of Ohio.

Open Access This article is distributed under the terms of the Creative Commons Attribution License which permits any use, distribution, and reproduction in any medium, provided the original author(s) and the source are credited.

References

1. M. Aguilar-Benitez et al. (LEBC-EHS Collaboration), Inclusive particle production in 400 GeV/ c pp-interactions. *Z. Phys. C* **50**, 405 (1991)
2. H. Albrecht et al., Inclusive production of $K^*(892)$, $\rho^0(770)$, and $\omega(783)$ mesons in the Υ energy region. *Z. Phys. C* **61**, 1 (1994)
3. J. Adams et al. (STAR Collaboration), $K(892)^*$ resonance production in Au+Au and p+p collisions at $\sqrt{s_{NN}} = 200$ GeV. *Phys. Rev. C* **71**, 064902 (2005)
4. S.S. Adler et al. (PHENIX Collaboration), Production of ϕ mesons at mid-rapidity in $\sqrt{s_{NN}} = 200$ -GeV Au+Au collisions at RHIC. *Phys. Rev. C* **72**, 014903 (2005)
5. B.I. Abelev et al. (STAR Collaboration), Measurements of ϕ meson production in relativistic heavy-ion collisions in the BNL Relativistic Heavy Ion Collider (RHIC). *Phys. Rev. C* **79**, 064903 (2009)
6. P.K. Malhotra, R. Orava, Determination of strange quark suppression in hadronic vacuum. *Z. Phys. C* **17**, 85 (1983)
7. A. Wroblewski, On the strange quark suppression factor in high energy collisions. *Acta Phys. Pol. B* **16**, 379 (1985)
8. V. Topor Pop et al., Strong longitudinal color-field effects in pp collisions at energies available at the CERN Large Hadron Collider. *Phys. Rev. C* **83**, 024902 (2011)
9. R. Engel, Photoproduction within the two component dual parton model. Amplitudes and cross-sections. *Z. Phys. C* **66**, 203 (1995)
10. R. Engel, J. Ranft, Hadronic photon-photon interactions at high-energies. *Phys. Rev. D* **54**, 4244 (1996)
11. T. Sjöstrand, S. Mrenna, P. Skands, PYTHIA 6.4 physics and manual. *J. High Energy Phys.* **05**, 026 (2006)

12. B. Abelev et al. (ALICE Collaboration), Measurement of pion, kaon and proton production in pp collisions at 7 TeV (in preparation)
13. B. Abelev et al. (ALICE Collaboration), Multi-strange baryon production in pp collisions at $\sqrt{s} = 7$ TeV with ALICE. *Phys. Lett. B* **712**, 309 (2012)
14. N. Armesto et al., Heavy-ion collisions at the LHC—last call for predictions. *J. Phys. G, Nucl. Part. Phys.* **35**, 054001 (2008)
15. P.Z. Skands, Tuning Monte Carlo generators: the Perugia tunes. *Phys. Rev. D* **82**, 074018 (2010)
16. K. Aamodt et al. (ALICE Collaboration), The ALICE experiment at the CERN LHC. *J. Instrum.* **3**, S08002 (2008)
17. K. Aamodt et al. (ALICE Collaboration), Alignment of the ALICE Inner Tracking System with cosmic-ray tracks. *J. Instrum.* **5**, P03003 (2010)
18. J. Alme et al., The ALICE TPC, a large 3-dimensional tracking device with fast readout for ultra-high multiplicity events. *Nucl. Instrum. Methods Phys. Res. A* **622**, 316 (2010)
19. A. Akindinov et al., The ALICE Time-Of-Flight system: Construction, assembly and quality tests. *Nuovo Cimento B* **124**, 235 (2009)
20. A. Akindinov et al., Results of the ALICE time-of-flight detector from the 2009 cosmic-ray data taking. *Eur. Phys. J. C* **68**, 601 (2010)
21. B. Abelev et al. (ALICE Collaboration), Measurement of inelastic, single- and double-diffraction cross sections in proton-proton collisions at LHC with ALICE. [arXiv:1208.4968v1](https://arxiv.org/abs/1208.4968v1)
22. K. Aamodt et al. (ALICE Collaboration), First proton-proton collisions at the LHC as observed with the ALICE detector: Measurement of the charged particle pseudorapidity density at $\sqrt{s} = 900$ -GeV. *Eur. Phys. J. C* **65**, 111 (2010)
23. B. Alessandro et al. (ALICE Collaboration), ALICE: physics performance report, volume II. *J. Phys. G, Nucl. Part. Phys.* **32**, 1295 (2006)
24. W. Blum, W. Riegler, L. Rolandi, *Particle Detection with Drift Chambers*, 2nd edn., vol. 448 (Springer, Berlin, 2008)
25. K. Aamodt et al. (ALICE Collaboration), Production of pions, kaons and protons in pp collisions at $\sqrt{s} = 900$ GeV with ALICE at the LHC. *Eur. Phys. J. C* **71**, 1655 (2011)
26. K. Nakamura et al. (Particle Data Group), Review of particle physics. *J. Phys. G* **37**, 075021 (2010) and 2011 partial update for the 2012 edition
27. C. Tsallis, Possible generalization of Boltzmann-Gibbs statistics. *J. Stat. Phys.* **52**, 479 (1988)
28. B.I. Abelev et al. (STAR Collaboration), Strange particle production in p+p collisions at $\sqrt{s} = 200$ -GeV. *Phys. Rev. C* **75**, 064901 (2007)
29. A. Adare et al. (PHENIX Collaboration), Measurement of neutral mesons in p+p collisions at $\sqrt{s} = 200$ GeV and scaling properties of hadron production. *Phys. Rev. D* **83**, 052004 (2011)
30. K. Aamodt et al. (ALICE Collaboration), Charged-particle multiplicity measurement in proton-proton collisions at $\sqrt{s} = 0.9$ and 2.36 TeV with ALICE at LHC. *Eur. Phys. J. C* **68**, 89 (2010)
31. K. Aamodt et al. (ALICE Collaboration), Charged-particle multiplicity measurement in proton-proton collisions at $\sqrt{s} = 7$ TeV with ALICE at LHC. *Eur. Phys. J. C* **68**, 345 (2010)
32. B. Abelev et al. (ALICE Collaboration), Light vector meson production in pp collisions at $\sqrt{s} = 7$ TeV. *Phys. Lett. B* **710**, 557 (2012)
33. K. Aamodt et al. (ALICE Collaboration), Strange particle production in proton-proton collisions at $\sqrt{s} = 0.9$ TeV with ALICE at the LHC. *Eur. Phys. J. C* **71**, 1594 (2011)
34. T. Alexopoulos et al. (E735 Collaboration), ϕ meson production from $p\bar{p}$ collisions at $\sqrt{s} = 1.8$ TeV. *Z. Phys. C* **67**, 411 (1995)
35. B. Andersson et al., Parton fragmentation and string dynamics. *Phys. Rep.* **97**, 31 (1983)
36. R. Field, Physics at the Tevatron. *Acta Phys. Pol. B* **39**, 2611 (2008)
37. R. Field, Studying the underlying events at CDF and the LHC, in *Proceedings of the First International Workshop on Multiple Partonic Interactions at the LHC (MPI08)*, Perugia, Italy, 27–31 October 2008, p. 12. [arXiv:1003.4220](https://arxiv.org/abs/1003.4220)
38. C. Buttar et al., Simulations of minimum bias events and the underlying event, MC tuning and predictions for the LHC. *Acta Phys. Pol. B* **35**, 433 (2004)
39. S. Chatrchyan et al. (CMS Collaboration), Charged particle transverse momentum spectra in pp collisions at $\sqrt{s} = 0.9$ and 7 TeV. *J. High Energy Phys.* **08**, 086 (2011)
40. C. Markert, Resonance production in heavy ion collisions. *J. Phys. G, Nucl. Part. Phys.* **31**, S897 (2005)
41. M. Bleicher, J. Aichelin, Strange resonance production: probing chemical and thermal freezeout in relativistic heavy ion collisions. *Phys. Lett. B* **530**, 81 (2002)
42. F. Becattini, M. Gazdzicki, J. Sollfrank, On chemical equilibrium in nuclear collisions. *Eur. Phys. J. C* **5**, 143 (1998)
43. Y. Pei, A simple approach to describe hadron production rates in e^+e^- annihilation. *Z. Phys. C* **72**, 39 (1996)
44. H. Hofmann et al., Particle composition in hadronic jets in e^+e^- annihilation. *Annu. Rev. Nucl. Part. Sci.* **38**, 279 (1988)
45. C. Bocquet et al., A study of particle ratios and strangeness suppression in $p\bar{p}$ collisions at $\sqrt{s} = 630$ GeV with UA1. *Phys. Lett. B* **366**, 447 (1996)
46. F. Becattini et al., Features of particle multiplicities and strangeness production in central heavy ion collisions between 1.7A and 158A GeV/c. *Phys. Rev. C* **64**, 024901 (2001)
47. V. Blobel et al., Test of the Zweig selection rule in ϕ production by pp collisions. *Phys. Lett. B* **59**, 88 (1975)
48. K. Abe et al., Production of π^+ , K^+ , K^0 , K^{*0} , ϕ , p and Λ^0 in hadronic Z^0 decays. *Phys. Rev. D* **59**, 052001 (1999)
49. D. Drijard et al., Production of vector and tensor mesons in proton-proton collisions at $\sqrt{s} = 52.5$ GeV. *Z. Phys. C* **9**, 293 (1981)
50. T. Akesson et al., Inclusive vector-meson production in the central region of pp collisions at $\sqrt{s} = 63$ GeV. *Nucl. Phys. B* **203**, 27 (1982)
51. M.M. Aggarwal et al. (STAR Collaboration), K^{*0} production in Cu+Cu and Au+Au collisions at $\sqrt{s_{NN}} = 62.4$ GeV and 200 GeV. *Phys. Rev. C* **84**, 034909 (2011)
52. C. Adler et al. (STAR Collaboration), Midrapidity ϕ production in Au+Au collisions at $\sqrt{s_{NN}} = 130$ GeV. *Phys. Rev. C* **65**, 041901 (2002)
53. C. Adler et al. (STAR Collaboration), $K^*(892)^0$ production in relativistic heavy ion collisions at $\sqrt{s_{NN}} = 130$ GeV. *Phys. Rev. C* **66**, 061901 (2002)
54. B.B. Back et al. (E917 Collaboration), Production of ϕ mesons in Au+Au collisions at 11.7A GeV/c. *Phys. Rev. C* **69**, 054901 (2004)
55. S.V. Afanasiev et al. (NA49 Collaboration), Production of ϕ -mesons in p+p, p+Pb and central Pb+Pb collisions at $E_{beam} = 158$ A GeV. *Phys. Lett. B* **491**, 59 (2000)
56. C. Alt et al. (NA49 Collaboration), Energy dependence of ϕ meson production in central Pb+Pb collision at $\sqrt{s_{NN}} = 6$ to 17 GeV. *Phys. Rev. C* **78**, 044907 (2008)
57. K. Adcox et al. (PHENIX Collaboration), Centrality dependence of $\pi^{+/-}$, $K^{+/-}$, p, and \bar{p} production from $\sqrt{s_{NN}} = 130$ GeV Au+Au collisions at RHIC. *Phys. Rev. Lett.* **88**, 242301 (2002)
58. J. Adams et al. (STAR Collaboration), Identified particle distributions in pp and Au+Au collisions at $\sqrt{s_{NN}} = 200$ GeV. *Phys. Rev. Lett.* **92**, 112301 (2004)
59. C. Daum et al., Inclusive ϕ -meson production in 93 and 63 hadron interactions. *Nucl. Phys. B* **186**, 205 (1981)
60. A.M. Rossi et al., Experimental study of the energy dependence in proton-proton inclusive reactions. *Nucl. Phys. B* **84**, 269 (1975)

61. A. Adare et al. (PHENIX Collaboration), Identified charged hadron production in p+p collisions at $\sqrt{s} = 200$ and 62.4 GeV. *Phys. Rev. C* **83**, 064903 (2011)
62. S. Behrends et al., Inclusive hadron production in upilon decay and nonresonant electron-positron annihilation at 10.49 GeV. *Phys. Rev. D* **31**, 2161 (1985)
63. D. Acosta et al. (CDF Collaboration), K_S^0 and Λ^0 production studies in $p\bar{p}$ collisions at $\sqrt{s} = 1800$ and 630 GeV/c. *Phys. Rev. D* **72**, 052001 (2005)
64. V. Topor Pop, private communication

The ALICE Collaboration

B. Abelev¹²⁵, J. Adam⁷⁵, D. Adamová¹⁰², A.M. Adare¹¹⁹, M.M. Aggarwal⁸⁷, G. Aglieri Rinella²⁴, A.G. Agocs¹²⁶, A. Agostinelli⁴⁷, S. Aguilar Salazar¹⁰³, Z. Ahammed⁵², A. Ahmad Masoodi²⁶, N. Ahmad²⁶, S.U. Ahn⁵⁴, A. Akindinov²⁸, D. Aleksandrov¹¹⁵, B. Alessandro⁹², R. Alfaro Molina¹⁰³, A. Alici^{60,117}, A. Alkin¹⁰⁵, E. Almaráz Aviña¹⁰³, J. Alme¹⁸, T. Alt⁵¹, V. Altini⁹⁷, S. Altinpinar⁸³, I. Altsybeev⁵⁸, C. Andrei⁴⁹, A. Andronic⁷³, V. Anguelov¹¹, J. Anielski⁹⁹, T. Antičić¹⁵, F. Antinori¹⁰⁴, P. Antonioli¹¹⁷, L. Aphecetche⁷⁸, H. Appelshäuser²⁰, N. Arbor⁵⁶, S. Arcelli⁴⁷, N. Armesto¹⁰⁶, R. Arnaldi⁹², T. Aronsson¹¹⁹, I.C. Arsene⁷³, M. Arslandok²⁰, A. Augustinus²⁴, R. Averbeck⁷³, T.C. Awes¹¹¹, J. Äystö²⁹, M.D. Azmi²⁶, M. Bach⁵¹, A. Badalá⁷⁴, Y.W. Baek^{5,54}, R. Bailhache²⁰, R. Bala⁹², R. Baldini Ferroli⁶⁰, A. Baldisseri¹²³, A. Baldit⁵, F. Baltasar Dos Santos Pedrosa²⁴, J. Bán⁸⁴, R.C. Baral⁹¹, R. Barbera⁸¹, F. Barile⁹⁷, G.G. Barnaföldi¹²⁶, L.S. Barnby³¹, V. Barret⁵, J. Bartke¹⁴, M. Basile⁴⁷, N. Bastid⁵, S. Basu⁵², B. Bathen⁹⁹, G. Batigne⁷⁸, B. Batyunya³⁸, C. Baumann²⁰, I.G. Bearden¹¹⁶, H. Beck²⁰, N.K. Behera¹²⁴, I. Belikov⁹⁸, F. Bellini⁴⁷, R. Bellwied⁶⁹, E. Belmont-Moreno¹⁰³, G. Bencedi¹²⁶, S. Beole²⁵, I. Berceanu⁴⁹, A. Bercuci⁴⁹, Y. Berdnikov⁸⁸, D. Berenyi¹²⁶, A.A.E. Bergognon⁷⁸, D. Berzano⁹², L. Betev²⁴, A. Bhasin³⁷, A.K. Bhati⁸⁷, J. Bhom⁶², L. Bianchi²⁵, N. Bianchi⁹, C. Bianchin³, J. Bielčik⁷⁵, J. Bielčiková¹⁰², A. Bilandžić¹¹⁶, S. Bjelogrić², F. Blanco⁵⁵, F. Blanco⁶⁹, D. Blau¹¹⁵, C. Blume²⁰, N. Bock⁵⁹, S. Böttger⁵⁷, A. Bogdanov¹⁶, H. Bøggild¹¹⁶, M. Bogolyubsky⁴⁵, L. Boldizsár¹²⁶, M. Bombara¹³, J. Book²⁰, H. Borel¹²³, A. Borissov⁹⁴, S. Bose¹², F. Bossú²⁵, M. Botje³², B. Boyer³⁵, E. Braidot¹⁰, P. Braun-Munzinger⁷³, M. Bregant⁷⁸, T. Breitner⁵⁷, T.A. Browning⁹⁶, M. Broz⁶³, R. Brun²⁴, E. Bruna⁹², G.E. Bruno⁹⁷, D. Budnikov⁹³, H. Buesching²⁰, S. Bufalino⁹², O. Busch¹¹, Z. Buthelezi⁸⁹, D. Caffarri³, X. Cai⁶⁶, H. Caines¹¹⁹, E. Calvo Villar³³, P. Camerini³⁰, V. Canoa Roman⁴⁸, G. Cara Romeo¹¹⁷, F. Carena²⁴, W. Carena²⁴, F. Carminati²⁴, A. Casanova Díaz⁹, J. Castillo Castellanos¹²³, E.A.R. Casula⁶¹, V. Catanescu⁴⁹, C. Cavicchioli²⁴, C. Ceballos Sanchez⁷¹, J. Cepila⁷⁵, P. Cerello⁹², B. Chang²⁹, S. Chapeland²⁴, J.L. Charvet¹²³, S. Chattopadhyay¹², S. Chattopadhyay⁵², I. Chawla⁸⁷, M. Cherney¹¹², C. Cheshkov³⁹, B. Cheynis³⁹, E. Chiavassa⁹², V. Chibante Barroso²⁴, D.D. Chinellato¹¹³, P. Chochula²⁴, M. Chojnacki², S. Choudhury⁵², P. Christakoglou³², C.H. Christensen¹¹⁶, P. Christiansen¹⁰⁷, T. Chujo⁶², S.U. Chung⁷⁶, C. Cicalo²⁷, L. Cifarelli^{47,60}, F. Cindolo¹¹⁷, J. Cleymans⁸⁹, F. Coccetti⁶⁰, F. Colamaria⁹⁷, D. Colella⁹⁷, G. Conesa Balbastre⁵⁶, Z. Conesa del Valle²⁴, P. Constantin¹¹, G. Contin³⁰, J.G. Contreras⁴⁸, T.M. Cormier⁹⁴, Y. Corrales Morales²⁵, I. Cortés Maldonado⁷⁷, P. Cortese¹¹⁸, M.R. Cosentino¹⁰, F. Costa²⁴, M.E. Cotallo⁵⁵, P. Crochet⁵, E. Cruz Alaniz¹⁰³, E. Cuautle⁷², L. Cunqueiro⁹, G. D Erasmo⁹⁷, A. Dainese¹⁰⁴, H.H. Dalsgaard¹¹⁶, A. Danu³⁶, D. Das¹², I. Das³⁵, K. Das¹², A. Dash¹¹³, S. Dash¹²⁴, S. De⁵², G.O.V. de Barros⁴⁶, A. De Caro^{60,42}, G. de Cataldo⁹⁰, J. de Cuveland⁵¹, A. De Falco⁶¹, D. De Gruttola⁴², N. De Marco⁹², S. De Pasquale⁴², R. de Rooij², H. Delagrange⁷⁸, A. Deloff⁸², V. Demanov⁹³, E. Dénes¹²⁶, A. Deppman⁴⁶, D. Di Bari⁹⁷, C. Di Giglio⁹⁷, S. Di Liberto¹⁰⁰, A. Di Mauro²⁴, P. Di Nezza⁹, M.A. Diaz Corchero⁵⁵, T. Dietel⁹⁹, R. Divià²⁴, Ø. Djuvsland⁸³, A. Dobrin⁹⁴, T. Dobrowolski⁸², I. Domínguez⁷², B. Dönigus⁷³, O. Dordic²¹, O. Driga⁷⁸, A.K. Dubey⁵², A. Dubla², L. Ducroux³⁹, P. Dupieux⁵, A.K. Dutta Majumdar¹², M.R. Dutta Majumdar⁵², D. Elia⁹⁰, D. Emschermann⁹⁹, H. Engel⁵⁷, B. Erazmus⁷⁸, H.A. Erdal¹⁸, B. Espagnon³⁵, M. Estienne⁷⁸, S. Esumi⁶², D. Evans³¹, G. Eyyubova²¹, D. Fabris¹⁰⁴, J. Faivre⁵⁶, D. Falchieri⁴⁷, A. Fantoni⁹, M. Fasel⁷³, A. Fedunov³⁸, D. Fehlkner⁸³, L. Feldkamp⁹⁹, D. Felea³⁶, B. Fenton-Olsen¹⁰, G. Feofilov⁵⁸, A. Fernández Téllez⁷⁷, A. Ferretti²⁵, R. Ferretti¹¹⁸, A. Festanti³, J. Figiel¹⁴, M.A.S. Figueredo⁴⁶, S. Filchagin⁹³, D. Finogeev⁸⁰, F.M. Fionda⁹⁷, E.M. Fiore⁹⁷, M. Floris²⁴, S. Foertsch⁸⁹, P. Foka⁷³, S. Fokin¹¹⁵, E. Fragiacomo¹⁰⁸, A. Francescon^{24,3}, U. Frankenfeld⁷³, U. Fuchs²⁴, C. Furget⁵⁶, M. Fusco Girard⁴², J.J. Gaardhøje¹¹⁶, M. Gagliardi²⁵, A. Gago³³, M. Gallio²⁵, D.R. Gangadharan⁵⁹, P. Ganoti¹¹¹, C. Garabatos⁷³, E. Garcia-Solis¹²⁰, I. Garishvili¹²⁵, J. Gerhard⁵¹, M. Germain⁷⁸, C. Geuna¹²³, A. Gheata²⁴, M. Gheata^{24,36}, B. Ghidini⁹⁷, P. Ghosh⁵², P. Gianotti⁹, M.R. Girard⁹⁵, P. Giubellino²⁴, E. Gladysz-Dziadus¹⁴, P. Glässel¹¹, R. Gomez⁶⁷, E.G. Ferreira¹⁰⁶, L.H. González-Trueba¹⁰³, P. González-Zamora⁵⁵, S. Gorbunov⁵¹, A. Goswami⁵³, S. Gotovac¹¹⁴, V. Grabski¹⁰³, L.K. Graczykowski⁹⁵, R. Grajcarek¹¹, A. Grelli², A. Grigoras²⁴, C. Grigoras²⁴, V. Grigoriev¹⁶, A. Grigoryan⁷, S. Grigoryan³⁸, B. Grinyov¹⁰⁵, N. Grión¹⁰⁸, J.F. Grosse-Oetringhaus²⁴, J.-Y. Grossiord³⁹, R. Grosso²⁴, F. Guber⁸⁰, R. Guernane⁵⁶, C. Guerra Gutierrez³³, B. Guerzoni⁴⁷, M. Guilbaud³⁹, K. Gulbrandsen¹¹⁶, T. Gunji²², A. Gupta³⁷, R. Gupta³⁷,

H. Gutbrod⁷³, Ø. Haaland⁸³, C. Hadjidakis³⁵, M. Haiduc³⁶, H. Hamagaki²², G. Hamar¹²⁶, L.D. Hanratty³¹, A. Hansen¹¹⁶, Z. Harmanova¹³, J.W. Harris¹¹⁹, M. Hartig²⁰, D. Hasegan³⁶, D. Hatzifotiadou¹¹⁷, A. Hayrapetyan^{7,24}, S.T. Heckel²⁰, M. Heide⁹⁹, H. Helstrup¹⁸, A. Hergehelegiu⁴⁹, G. Herrera Corral⁴⁸, N. Herrmann¹¹, B.A. Hess¹, K.F. Hetland¹⁸, B. Hicks¹¹⁹, P.T. Hille¹¹⁹, B. Hippolyte⁹⁸, T. Horaguchi⁶², Y. Hori²², P. Hristov²⁴, I. Hřivnáčová³⁵, M. Huang⁸³, T.J. Humanic⁵⁹, D.S. Hwang⁶⁵, R. Ichou⁵, R. Ilkaev⁹³, I. Ilkiv⁸², M. Inaba⁶², E. Incani⁶¹, G.M. Innocenti²⁵, M. Ippolitov¹¹⁵, M. Irfan²⁶, C. Ivan⁷³, A. Ivanov⁵⁸, M. Ivanov⁷³, V. Ivanov⁸⁸, O. Ivanytskyi¹⁰⁵, A. Jacholkowski⁸¹, P. M. Jacobs¹⁰, M.A. Janik⁹⁵, R. Janik⁶³, P.H.S.Y. Jayarathna⁶⁹, S. Jena¹²⁴, D.M. Jha⁹⁴, R.T. Jimenez Bustamante⁷², L. Jirde²⁴, P.G. Jones³¹, H. Jung⁵⁴, A. Jusko³¹, V. Kakoyan⁷, S. Kalcher⁵¹, P. Kaliňák⁸⁴, T. Kalliokoski²⁹, A. Kalweit^{24,86}, J.H. Kang⁶, V. Kaplin¹⁶, A. Karasu Uysal²⁴, O. Karavichev⁸⁰, T. Karavicheva⁸⁰, E. Karpechev⁸⁰, A. Kazantsev¹¹⁵, U. Kebschull⁵⁷, R. Keidel⁶⁸, M.M. Khan²⁶, P. Khan¹², S.A. Khan⁵², A. Khanzadeev⁸⁸, Y. Kharlov⁴⁵, B. Kileng¹⁸, B. Kim⁶, D.J. Kim²⁹, D.W. Kim⁵⁴, J.H. Kim⁶⁵, J.S. Kim⁵⁴, M. Kim⁶, M. Kim⁵⁴, S. Kim⁶⁵, S.H. Kim⁵⁴, T. Kim⁶, S. Kirsch⁵¹, I. Kisel⁵¹, S. Kiselev²⁸, A. Kisiel⁹⁵, J.L. Klay⁴⁰, J. Klein¹¹, C. Klein-Bösing⁹⁹, A. Kluge²⁴, M.L. Knichel⁷³, A.G. Knospe⁷⁹, K. Koch¹¹, M.K. Köhler⁷³, T. Kollegger⁵¹, A. Kolojvari⁵⁸, V. Kondratiev⁵⁸, N. Kondratyeva¹⁶, A. Konevskikh⁸⁰, A. Korneev⁹³, R. Kour³¹, M. Kowalski¹⁴, S. Kox⁵⁶, G. Koyithatta Meethalevedu¹²⁴, J. Kral²⁹, I. Králik⁸⁴, F. Kramer²⁰, I. Kraus⁷³, T. Krawutschke^{11,121}, M. Krelina⁷⁵, M. Kretz⁵¹, M. Krivda^{31,84}, F. Krizek²⁹, M. Krus⁷⁵, E. Kryshen⁸⁸, M. Krzewicki⁷³, Y. Kucheriaev¹¹⁵, T. Kugathasan²⁴, C. Kuhn⁹⁸, P.G. Kuijer³², I. Kulakov²⁰, J. Kumar¹²⁴, P. Kurashvili⁸², A. Kurepin⁸⁰, A.B. Kurepin⁸⁰, A. Kuryakin⁹³, S. Kushpil¹⁰², V. Kushpil¹⁰², M.J. Kweon¹¹, Y. Kwon⁶, S.L. La Pointe², P. La Rocca⁸¹, P. Ladrón de Guevara⁷², I. Lakomov³⁵, R. Langoy⁸³, C. Lara⁵⁷, A. Lardeux⁷⁸, C. Lazzeroni³¹, Y. Le Bornec³⁵, R. Lea³⁰, M. Lechman²⁴, G.R. Lee³¹, K.S. Lee⁵⁴, S.C. Lee⁵⁴, F. Lefèvre⁷⁸, J. Lehnert²⁰, L. Leistam²⁴, R.C. Lemmon¹⁹, V. Lenti⁹⁰, I. León Monzón⁶⁷, H. León Vargas²⁰, M. Leoncino⁹², P. Lévai¹²⁶, J. Lien⁸³, R. Lietava³¹, S. Lindal²¹, V. Lindenstruth⁵¹, C. Lippmann⁷³, M.A. Lisa⁵⁹, L. Liu⁸³, V.R. Loggins⁹⁴, V. Loginov¹⁶, S. Lohn²⁴, D. Lohner¹¹, C. Loizides¹⁰, K.K. Loo²⁹, X. Lopez⁵, E. López Torres⁷¹, G. Løvhøiden²¹, X.-G. Lu¹¹, P. Luettig²⁰, M. Lunardon³, J. Luo⁶⁶, G. Luparello², L. Luquin⁷⁸, C. Luzzi²⁴, R. Ma¹¹⁹, A. Maevskaya⁸⁰, M. Mager²⁴, D.P. Mahapatra⁹¹, A. Maire¹¹, D. Mal'Kevich²⁸, M. Malaev⁸⁸, I. Maldonado Cervantes⁷², L. Malinina^{38,a}, P. Malzacher⁷³, A. Mamonov⁹³, L. Manceau⁹², V. Manko¹¹⁵, F. Manso⁵, V. Manzari⁹⁰, Y. Mao⁶⁶, M. Marchisone^{25,5}, J. Mareš²³, G.V. Margagliotti³⁰, A. Margotti¹¹⁷, A. Marín⁷³, C.A. Marin Tobon²⁴, C. Markert⁷⁹, I. Martashvili⁴⁴, P. Martinengo²⁴, M.I. Martínez⁷⁷, A. Martínez Davalos¹⁰³, G. Martínez García⁷⁸, Y. Martynov¹⁰⁵, A. Mas⁷⁸, S. Masciocchi⁷³, M. Masera²⁵, A. Masoni²⁷, A. Mastroserio⁹⁷, Z.L. Matthews³¹, A. Matyja^{78,14}, C. Mayer¹⁴, J. Mazer⁴⁴, M.A. Mazzoni¹⁰⁰, F. Meddi⁴³, A. Menchaca-Rocha¹⁰³, J. Mercado Pérez¹¹, M. Meres⁶³, Y. Miake⁶², L. Milano²⁵, J. Milosevic^{21,b}, A. Mischke², A.N. Mishra⁵³, D. Miśkowiec^{24,73}, C. Mitu³⁶, J. Mlynarz⁹⁴, B. Mohanty⁵², L. Molnar^{24,126}, L. Montaña Zetina⁴⁸, M. Monteno⁹², E. Montes⁵⁵, T. Moon⁶, M. Morando³, D.A. Moreira De Godoy⁴⁶, S. Moretto³, A. Morsch²⁴, V. Muccifora⁹, E. Mudnic¹¹⁴, S. Muhuri⁵², M. Mukherjee⁵², H. Müller²⁴, M.G. Munhoz⁴⁶, L. Musa²⁴, A. Musso⁹², B.K. Nandi¹²⁴, R. Nania¹¹⁷, E. Nappi⁹⁰, C. Nattrass⁴⁴, N.P. Naumov⁹³, S. Navin³¹, T.K. Nayak⁵², S. Nazarenko⁹³, G. Nazarov⁹³, A. Nedosekin²⁸, M. Nicassio⁹⁷, M. Niculescu^{36,24}, B.S. Nielsen¹¹⁶, T. Niida⁶², S. Nikolaev¹¹⁵, S. Nikulin¹¹⁵, V. Nikulin⁸⁸, B.S. Nilsen¹¹², M.S. Nilsson²¹, F. Noferini^{60,117}, P. Nomokonov³⁸, G. Nooren², N. Novitzky²⁹, A. Nyanin¹¹⁵, A. Nyatha¹²⁴, C. Nygaard¹¹⁶, J. Nystrand⁸³, H. Oeschler⁸⁶, S. Oh¹¹⁹, S.K. Oh⁵⁴, J. Oleniacz⁹⁵, C. Oppedisano⁹², G. Ortona²⁵, A. Oskarsson¹⁰⁷, J. Otwinowski⁷³, K. Oyama¹¹, Y. Pachmayer¹¹, M. Pachr⁷⁵, F. Padilla²⁵, P. Pagano⁴², G. Paic⁷², F. Painke⁵¹, C. Pajares¹⁰⁶, S.K. Pal⁵², A. Palaha³¹, A. Palmeri⁷⁴, V. Papikyan⁷, G.S. Pappalardo⁷⁴, W.J. Park⁷³, A. Passfeld⁹⁹, D.I. Patalakha⁴⁵, V. Paticchio⁹⁰, A. Pavlinov⁹⁴, T. Pawlak⁹⁵, T. Peitzmann², H. Pereira Da Costa¹²³, E. Pereira De Oliveira Filho⁴⁶, D. Pere-sunko¹¹⁵, C.E. Pérez Lara³², E. Perez Lezama⁷², D. Perini²⁴, D. Perrino⁹⁷, W. Peryt⁹⁵, A. Pesci¹¹⁷, V. Peskov²⁴, Y. Pestov⁴¹, V. Petráček⁷⁵, M. Petran⁷⁵, M. Petris⁴⁹, P. Petrov³¹, M. Petrovici⁴⁹, C. Petta⁸¹, S. Piano¹⁰⁸, A. Piccotti⁹², M. Pikna⁶³, P. Pillot⁷⁸, O. Pinazza²⁴, L. Pinsky⁶⁹, N. Pitz²⁰, F. Piuz²⁴, D.B. Piyarathna⁶⁹, M. Płoskoń¹⁰, J. Pluta⁹⁵, S. Pochybova¹²⁶, P.L.M. Podesta-Lerma⁶⁷, M.G. Poghosyan^{25,24}, B. Polichtchouk⁴⁵, A. Pop⁴⁹, S. Porteboeuf-Houssais⁵, V. Pospíšil⁷⁵, B. Potukuchi³⁷, S.K. Prasad⁹⁴, R. Preghenella^{60,117}, F. Prino⁹², C.A. Pruneau⁹⁴, I. Pshenichnov⁸⁰, S. Puchagin⁹³, G. Puddu⁶¹, P. Pujahari¹²⁴, A. Pulvirenti⁸¹, V. Punin⁹³, M. Putiš¹³, J. Putschke⁹⁴, E. Quercigh²⁴, H. Qvigstad²¹, A. Rachevski¹⁰⁸, A. Rademakers²⁴, T.S. Rähä²⁹, J. Rak²⁹, A. Rakotozafindrabe¹²³, L. Ramello¹¹⁸, A. Ramírez Reyes⁴⁸, R. Raniwala⁵³, S. Raniwala⁵³, S.S. Räsänen²⁹, B.T. Rascanu²⁰, D. Rathee⁸⁷, K.F. Read⁴⁴, J.S. Real⁵⁶, K. Redlich⁸², A. Rehman⁸³, P. Reichelt²⁰, M. Reicher², R. Renfordt²⁰, A.R. Reolon⁹, A. Reshetin⁸⁰, F. Rettig⁵¹, J.-P. Revol²⁴, K. Reygers¹¹, L. Riccati⁹², R.A. Ricci¹⁷, T. Richert¹⁰⁷, M. Richter²¹, P. Riedler²⁴, W. Riegler²⁴, F. Riggi⁸¹, B. Rodrigues Fernandes Rabacal²⁴, M. Rodríguez Cahuantzi⁷⁷, A. Rodriguez Manso³², K. Røed⁸³, D. Rohr⁵¹, D. Röhrich⁸³, R. Romita⁷³, F. Ronchetti⁹, P. Rosnet⁵, S. Rossegger²⁴, A. Rossi^{3,24}, C. Roy⁹⁸, P. Roy¹², A.J. Rubio Montero⁵⁵, R. Rui³⁰, R. Russo²⁵, E. Ryabinkin¹¹⁵, A. Rybicki¹⁴, S. Sadovsky⁴⁵, K. Šafařík²⁴, R. Sahoo⁷⁰, P.K. Sahu⁹¹, J. Saini⁵², H. Sakaguchi¹⁰⁹, S. Sakai¹⁰, D. Sakata⁶², C.A. Salgado¹⁰⁶, J. Salzwedel⁵⁹, S. Sambyal³⁷, V. Samsonov⁸⁸, X. Sanchez Castro⁹⁸, L. Šándor⁸⁴, A. Sandoval¹⁰³, M. Sano⁶², S. Sano²², R. Santo⁹⁹, R. Santoro^{24,60}, J. Sarkamo²⁹, E. Scapparone¹¹⁷, F. Scarlassara³, R.P. Scharenberg⁹⁶, C. Schiaua⁴⁹,

R. Schicker¹¹, C. Schmidt⁷³, H.R. Schmidt¹, S. Schreiner²⁴, S. Schuchmann²⁰, J. Schukraft²⁴, Y. Schutz^{78,24}, K. Schwarz⁷³, K. Schweda⁷³, G. Scioli⁴⁷, E. Scomparin⁹², P.A. Scott³¹, R. Scott⁴⁴, G. Segato³, I. Selyuzhenkov⁷³, S. Senyukov¹¹⁸, J. Seo⁷⁶, S. Serçi⁶¹, E. Serradilla^{103,55}, A. Sevcenco³⁶, A. Shabetai⁷⁸, G. Shabratova³⁸, R. Shahoyan²⁴, N. Sharma⁸⁷, S. Sharma³⁷, K. Shigaki¹⁰⁹, M. Shimomura⁶², K. Shtejer⁷¹, Y. Sibiraki¹¹⁵, M. Siciliano²⁵, E. Sicking²⁴, S. Siddhanta²⁷, T. Siemiarczuk⁸², D. Silvermyr¹¹¹, C. Silvestre⁵⁶, G. Simatovic¹⁵, G. Simonetti²⁴, R. Singaraju⁵², R. Singh³⁷, S. Singha⁵², V. Singhal⁵², B.C. Sinha⁵², T. Sinha¹², B. Sitar⁶³, M. Sitta¹¹⁸, T.B. Skaali²¹, K. Skjerdal⁸³, R. Smakal⁷⁵, N. Smirnov¹¹⁹, R.J.M. Snellings², C. Sogaard¹¹⁶, R. Soltz¹²⁵, H. Son⁶⁵, J. Song⁷⁶, M. Song⁶, C. Soos²⁴, F. Soramel³, I. Sputowska¹⁴, M. Spyropoulou-Stassinaki¹⁰¹, B.K. Srivastava⁹⁶, J. Stachel¹¹, I. Stan³⁶, G. Stefanek⁸², G. Stefanini²⁴, M. Steinpreis⁵⁹, E. Stenlund¹⁰⁷, G. Steyn⁸⁹, J.H. Stiller¹¹, D. Stocco⁷⁸, M. Stolpovskiy⁴⁵, K. Strabykin⁹³, P. Strmen⁶³, A.A.P. Suaide⁴⁶, M.A. Subieta Vásquez²⁵, T. Sugitate¹⁰⁹, C. Suire³⁵, M. Sukhorukov⁹³, R. Sultanov²⁸, M. Šumbera¹⁰², T. Susa¹⁵, A. Szanto de Toledo⁴⁶, I. Szarka⁶³, A. Szczepankiewicz¹⁴, A. Szostak⁸³, M. Szymański⁹⁵, J. Takahashi¹¹³, J.D. Tapia Takaki³⁵, A. Tarazona Martínez²⁴, A. Tauro²⁴, G. Tejeda Muñoz⁷⁷, A. Telesca²⁴, C. Terrevoli⁹⁷, J. Thäder⁷³, D. Thomas², R. Tieulent³⁹, A.R. Timmins⁶⁹, A. Toia^{51,3}, H. Torii²², F. Tosello⁹², V. Trubnikov¹⁰⁵, W.H. Trzaska²⁹, T. Tsuji²², A. Tumkin⁹³, R. Turrissi¹⁰⁴, T.S. Tveter²¹, J. Ulery²⁰, K. Ullaland⁸³, J. Ulrich⁵⁷, A. Uras³⁹, J. Urbán¹³, G.M. Urciuoli¹⁰⁰, G.L. Usai⁶¹, M. Vajzer¹⁰², M. Vala^{38,84}, L. Valencia Palomo³⁵, S. Vallero¹¹, N. van der Kolk³², M. van Leeuwen², P. Vande Vyvre²⁴, L. Vannucci¹⁷, A. Vargas⁷⁷, R. Varma¹²⁴, M. Vasileiou¹⁰¹, A. Vasiliev¹¹⁵, V. Vechernin⁵⁸, M. Veldhoen², M. Venaruzzo³⁰, E. Vercellin²⁵, S. Vergara⁷⁷, R. Vernet⁵⁰, M. Verweij², L. Vickovic¹¹⁴, G. Viesti³, O. Vikhlyantsev⁹³, Z. Vilakazi⁸⁹, O. Villalobos Bailie³¹, A. Vinogradov¹¹⁵, L. Vinogradov⁵⁸, Y. Vinogradov⁹³, T. Virgili⁴², Y.P. Viyogi⁵², A. Vodopyanov³⁸, K. Voloshin²⁸, S. Voloshin⁹⁴, G. Volpe²⁴, B. von Haller²⁴, D. Vranic⁷³, G. Øvrebeek⁸³, J. Vrláková¹³, B. Vulpescu⁵, A. Vyushin⁹³, B. Wagner⁸³, V. Wagner⁷⁵, R. Wan⁶⁶, D. Wang⁶⁶, M. Wang⁶⁶, Y. Wang¹¹, Y. Wang⁶⁶, K. Watanabe⁶², M. Weber⁶⁹, J.P. Wessels^{24,99}, U. Westerhoff⁹⁹, J. Wiechula¹, J. Wikne²¹, M. Wilde⁹⁹, A. Wilk⁹⁹, G. Wilk⁸², M.C.S. Williams¹¹⁷, B. Windelband¹¹, L. Xaplanteris Karampatsos⁷⁹, C.G. Yaldo⁹⁴, Y. Yamaguchi²², H. Yang¹²³, S. Yang⁸³, S. Yasnopolskiy¹¹⁵, J. Yi⁷⁶, Z. Yin⁶⁶, I.-K. Yoo⁷⁶, J. Yoon⁶, W. Yu²⁰, X. Yuan⁶⁶, I. Yushmanov¹¹⁵, C. Zach⁷⁵, C. Zampolli¹¹⁷, S. Zaporozhets³⁸, A. Zarochentsev⁵⁸, P. Závada²³, N. Zaviyalov⁹³, H. Zbroszczyk⁹⁵, P. Zelnicek⁵⁷, I.S. Zgura³⁶, M. Zhalov⁸⁸, H. Zhang⁶⁶, X. Zhang⁶⁶, D. Zhou⁶⁶, F. Zhou⁶⁶, Y. Zhou², J. Zhu⁶⁶, X. Zhu⁶⁶, A. Zichichi^{47,60}, A. Zimmermann¹¹, G. Zinovjev¹⁰⁵, Y. Zoccarato³⁹, M. Zynovyev¹⁰⁵, M. Zyzak²⁰

¹Eberhard Karls Universität Tübingen, Tübingen, Germany

²Nikhef, National Institute for Subatomic Physics and Institute for Subatomic Physics of Utrecht University, Utrecht, Netherlands

³Dipartimento di Fisica dell'Università and Sezione INFN, Padova, Italy

⁴COMSATS Institute of Information Technology (CIIT), Islamabad, Pakistan

⁵Laboratoire de Physique Corpusculaire (LPC), Clermont Université, Université Blaise Pascal, CNRS-IN2P3, Clermont-Ferrand, France

⁶Yonsei University, Seoul, South Korea

⁷Yerevan Physics Institute, Yerevan, Armenia

⁸Scientific Research Technological Institute of Instrument Engineering, Kharkov, Ukraine

⁹Laboratori Nazionali di Frascati, INFN, Frascati, Italy

¹⁰Lawrence Berkeley National Laboratory, Berkeley, California, United States

¹¹Physikalisches Institut, Ruprecht-Karls-Universität Heidelberg, Heidelberg, Germany

¹²Saha Institute of Nuclear Physics, Kolkata, India

¹³Faculty of Science, P.J. Šafárik University, Košice, Slovakia

¹⁴The Henryk Niewodniczanski Institute of Nuclear Physics, Polish Academy of Sciences, Cracow, Poland

¹⁵Rudjer Bošković Institute, Zagreb, Croatia

¹⁶Moscow Engineering Physics Institute, Moscow, Russia

¹⁷Laboratori Nazionali di Legnaro, INFN, Legnaro, Italy

¹⁸Faculty of Engineering, Bergen University College, Bergen, Norway

¹⁹Nuclear Physics Group, STFC Daresbury Laboratory, Daresbury, United Kingdom

²⁰Institut für Kernphysik, Johann Wolfgang Goethe-Universität Frankfurt, Frankfurt, Germany

²¹Department of Physics, University of Oslo, Oslo, Norway

²²University of Tokyo, Tokyo, Japan

²³Institute of Physics, Academy of Sciences of the Czech Republic, Prague, Czech Republic

²⁴European Organization for Nuclear Research (CERN), Geneva, Switzerland

²⁵Dipartimento di Fisica dell'Università and Sezione INFN, Turin, Italy

- ²⁶Department of Physics Aligarh Muslim University, Aligarh, India
- ²⁷Sezione INFN, Cagliari, Italy
- ²⁸Institute for Theoretical and Experimental Physics, Moscow, Russia
- ²⁹Helsinki Institute of Physics (HIP) and University of Jyväskylä, Jyväskylä, Finland
- ³⁰Dipartimento di Fisica dell'Università and Sezione INFN, Trieste, Italy
- ³¹School of Physics and Astronomy, University of Birmingham, Birmingham, United Kingdom
- ³²Nikhef, National Institute for Subatomic Physics, Amsterdam, Netherlands
- ³³Sección Física, Departamento de Ciencias, Pontificia Universidad Católica del Perú, Lima, Peru
- ³⁴Gauhati University, Department of Physics, Guwahati, India
- ³⁵Institut de Physique Nucléaire d'Orsay (IPNO), Université Paris-Sud, CNRS-IN2P3, Orsay, France
- ³⁶Institute of Space Sciences (ISS), Bucharest, Romania
- ³⁷Physics Department, University of Jammu, Jammu, India
- ³⁸Joint Institute for Nuclear Research (JINR), Dubna, Russia
- ³⁹Université de Lyon, Université Lyon 1, CNRS/IN2P3, IPN-Lyon, Villeurbanne, France
- ⁴⁰California Polytechnic State University, San Luis Obispo, California, United States
- ⁴¹Budker Institute for Nuclear Physics, Novosibirsk, Russia
- ⁴²Dipartimento di Fisica 'E.R. Caianiello' dell'Università and Gruppo Collegato INFN, Salerno, Italy
- ⁴³Dipartimento di Fisica dell'Università 'La Sapienza' and Sezione INFN, Rome, Italy
- ⁴⁴University of Tennessee, Knoxville, Tennessee, United States
- ⁴⁵Institute for High Energy Physics, Protvino, Russia
- ⁴⁶Universidade de São Paulo (USP), São Paulo, Brazil
- ⁴⁷Dipartimento di Fisica dell'Università and Sezione INFN, Bologna, Italy
- ⁴⁸Centro de Investigación y de Estudios Avanzados (CINVESTAV), Mexico City and Mérida, Mexico
- ⁴⁹National Institute for Physics and Nuclear Engineering, Bucharest, Romania
- ⁵⁰Centre de Calcul de l'IN2P3, Villeurbanne, France
- ⁵¹Frankfurt Institute for Advanced Studies, Johann Wolfgang Goethe-Universität Frankfurt, Frankfurt, Germany
- ⁵²Variable Energy Cyclotron Centre, Kolkata, India
- ⁵³Physics Department, University of Rajasthan, Jaipur, India
- ⁵⁴Gangneung-Wonju National University, Gangneung, South Korea
- ⁵⁵Centro de Investigaciones Energéticas Medioambientales y Tecnológicas (CIEMAT), Madrid, Spain
- ⁵⁶Laboratoire de Physique Subatomique et de Cosmologie (LPSC), Université Joseph Fourier, CNRS-IN2P3, Institut Polytechnique de Grenoble, Grenoble, France
- ⁵⁷Institut für Informatik, Johann Wolfgang Goethe-Universität Frankfurt, Frankfurt, Germany
- ⁵⁸V. Fock Institute for Physics, St. Petersburg State University, St. Petersburg, Russia
- ⁵⁹Department of Physics, Ohio State University, Columbus, Ohio, United States
- ⁶⁰Centro Fermi – Centro Studi e Ricerche e Museo Storico della Fisica "Enrico Fermi", Rome, Italy
- ⁶¹Dipartimento di Fisica dell'Università and Sezione INFN, Cagliari, Italy
- ⁶²University of Tsukuba, Tsukuba, Japan
- ⁶³Faculty of Mathematics, Physics and Informatics, Comenius University, Bratislava, Slovakia
- ⁶⁴Kirchhoff-Institut für Physik, Ruprecht-Karls-Universität Heidelberg, Heidelberg, Germany
- ⁶⁵Department of Physics, Sejong University, Seoul, South Korea
- ⁶⁶Hua-Zhong Normal University, Wuhan, China
- ⁶⁷Universidad Autónoma de Sinaloa, Culiacán, Mexico
- ⁶⁸Zentrum für Technologietransfer und Telekommunikation (ZTT), Fachhochschule Worms, Worms, Germany
- ⁶⁹University of Houston, Houston, Texas, United States
- ⁷⁰Indian Institute of Technology Indore (IIT), Indore, India
- ⁷¹Centro de Aplicaciones Tecnológicas y Desarrollo Nuclear (CEADEN), Havana, Cuba
- ⁷²Instituto de Ciencias Nucleares, Universidad Nacional Autónoma de México, Mexico City, Mexico
- ⁷³Research Division and ExtreMe Matter Institute EMMI, GSI Helmholtzzentrum für Schwerionenforschung, Darmstadt, Germany
- ⁷⁴Sezione INFN, Catania, Italy
- ⁷⁵Faculty of Nuclear Sciences and Physical Engineering, Czech Technical University in Prague, Prague, Czech Republic
- ⁷⁶Pusan National University, Pusan, South Korea

- ⁷⁷Benemérita Universidad Autónoma de Puebla, Puebla, Mexico
- ⁷⁸SUBATECH, Ecole des Mines de Nantes, Université de Nantes, CNRS-IN2P3, Nantes, France
- ⁷⁹The University of Texas at Austin, Physics Department, Austin, TX, United States
- ⁸⁰Institute for Nuclear Research, Academy of Sciences, Moscow, Russia
- ⁸¹Dipartimento di Fisica e Astronomia dell'Università and Sezione INFN, Catania, Italy
- ⁸²Soltan Institute for Nuclear Studies, Warsaw, Poland
- ⁸³Department of Physics and Technology, University of Bergen, Bergen, Norway
- ⁸⁴Institute of Experimental Physics, Slovak Academy of Sciences, Košice, Slovakia
- ⁸⁵Korea Institute of Science and Technology Information, Daejeon, South Korea
- ⁸⁶Institut für Kernphysik, Technische Universität Darmstadt, Darmstadt, Germany
- ⁸⁷Physics Department, Panjab University, Chandigarh, India
- ⁸⁸Petersburg Nuclear Physics Institute, Gatchina, Russia
- ⁸⁹Physics Department, University of Cape Town, iThemba LABS, Cape Town, South Africa
- ⁹⁰Sezione INFN, Bari, Italy
- ⁹¹Institute of Physics, Bhubaneswar, India
- ⁹²Sezione INFN, Turin, Italy
- ⁹³Russian Federal Nuclear Center (VNIIEF), Sarov, Russia
- ⁹⁴Wayne State University, Detroit, Michigan, United States
- ⁹⁵Warsaw University of Technology, Warsaw, Poland
- ⁹⁶Purdue University, West Lafayette, Indiana, United States
- ⁹⁷Dipartimento Interateneo di Fisica 'M. Merlin' and Sezione INFN, Bari, Italy
- ⁹⁸Institut Pluridisciplinaire Hubert Curien (IPHC), Université de Strasbourg, CNRS-IN2P3, Strasbourg, France
- ⁹⁹Institut für Kernphysik, Westfälische Wilhelms-Universität Münster, Münster, Germany
- ¹⁰⁰Sezione INFN, Rome, Italy
- ¹⁰¹Physics Department, University of Athens, Athens, Greece
- ¹⁰²Nuclear Physics Institute, Academy of Sciences of the Czech Republic, Řež u Prahy, Czech Republic
- ¹⁰³Instituto de Física, Universidad Nacional Autónoma de México, Mexico City, Mexico
- ¹⁰⁴Sezione INFN, Padova, Italy
- ¹⁰⁵Bogolyubov Institute for Theoretical Physics, Kiev, Ukraine
- ¹⁰⁶Departamento de Física de Partículas and IGFAE, Universidad de Santiago de Compostela, Santiago de Compostela, Spain
- ¹⁰⁷Division of Experimental High Energy Physics, University of Lund, Lund, Sweden
- ¹⁰⁸Sezione INFN, Trieste, Italy
- ¹⁰⁹Hiroshima University, Hiroshima, Japan
- ¹¹⁰Bose Institute, Department of Physics and Centre for Astroparticle Physics and Space Science (CAPSS), Kolkata, India
- ¹¹¹Oak Ridge National Laboratory, Oak Ridge, Tennessee, United States
- ¹¹²Physics Department, Creighton University, Omaha, Nebraska, United States
- ¹¹³Universidade Estadual de Campinas (UNICAMP), Campinas, Brazil
- ¹¹⁴Technical University of Split FESB, Split, Croatia
- ¹¹⁵Russian Research Centre Kurchatov Institute, Moscow, Russia
- ¹¹⁶Niels Bohr Institute, University of Copenhagen, Copenhagen, Denmark
- ¹¹⁷Sezione INFN, Bologna, Italy
- ¹¹⁸Dipartimento di Scienze e Innovazione Tecnologica dell'Università del Piemonte Orientale and Gruppo Collegato INFN, Alessandria, Italy
- ¹¹⁹Yale University, New Haven, Connecticut, United States
- ¹²⁰Chicago State University, Chicago, United States
- ¹²¹Fachhochschule Köln, Köln, Germany
- ¹²²China Institute of Atomic Energy, Beijing, China
- ¹²³Commissariat à l'Energie Atomique, IRFU, Saclay, France
- ¹²⁴Indian Institute of Technology, Mumbai, India
- ¹²⁵Lawrence Livermore National Laboratory, Livermore, California, United States
- ¹²⁶KFKI Research Institute for Particle and Nuclear Physics, Hungarian Academy of Sciences, Budapest, Hungary
- ^aAlso at: M.V.Lomonosov Moscow State University, D.V.Skobel'tsyn Institute of Nuclear Physics, Moscow, Russia
- ^bAlso at: University of Belgrade, Faculty of Physics and "Vinča" Institute of Nuclear Sciences, Belgrade, Serbia